Desalination 404 (2017) 230–248

Contents lists available at ScienceDirect

Desalination

journal homepage: www.elsevier.com/locate/desal

Shale gas flowback water desalination: Single *vs* multiple-effect evaporation with vapor recompression cycle and thermal integration

Viviani C. Onishi [a,*], Alba Carrero-Parreño [a], Juan A. Reyes-Labarta [a], Rubén Ruiz-Femenia [a], Raquel Salcedo-Díaz [a], Eric S. Fraga [b], José A. Caballero [a]

[a] Department of Chemical Engineering, University of Alicante, Ap. Correos 99, 03080 Alicante, Spain
[b] Centre for Process Systems Engineering, Department of Chemical Engineering, University College London, London WC1E 7JE, UK

HIGHLIGHTS

- New NLP model for the SEE/MEE systems design including MVR and thermal integration
- SEE/MEE model application to the high-salinity shale gas flowback water treatment.
- Optimization by minimizing costs to achieve brine salinity close to ZLD conditions.
- Sensitivity analysis to assess the system performance in distinct feed salinities
- Results highlight the model accuracy to cost-effectively synthesize SEE/MEE systems.

ARTICLE INFO

Article history:
Received 24 May 2016
Received in revised form 26 September 2016
Accepted 4 November 2016
Available online 22 November 2016

Keywords:
Shale gas
Single-effect evaporation (SEE)
Multiple-effect evaporation (MEE)
Mechanical vapor recompression (MVR)
Thermal integration
Zero liquid discharge (ZLD)

ABSTRACT

This paper introduces a new optimization model for the single and multiple-effect evaporation (SEE/MEE) systems design, including vapor recompression cycle and thermal integration. The SEE/MEE model is specially developed for shale gas flowback water desalination. A superstructure is proposed to solve the problem, comprising several evaporation effects coupled with intermediate flashing tanks that are used to enhance thermal integration by recovering condensate vapor. Multistage equipment with intercooling is used to compress the vapor formed by flashing and evaporation. The compression cycle is driven by electricity to operate on the vapor originating from the SEE/MEE system, providing all the energy needed in the process. The mathematical model is formulated as a nonlinear programming (NLP) problem optimized under GAMS software by minimizing the total annualized cost. The SEE/MEE system application for zero liquid discharge (ZLD) is investigated by allowing brine salinity discharge near to salt saturation conditions. Additionally, sensitivity analysis is carried out to evaluate the optimal process configuration and performance under distinct feed water salinity conditions. The results highlight the potential of the proposed model to cost-effectively optimize SEE/MEE systems by producing fresh water and reducing brine discharges and associated environmental impacts.

1. Introduction

Natural gas extracted from tight shale formations or "shale gas", is expected to play an important role in meeting the rising global energy demand. In the U.S., it is estimated that natural gas production from shale deposits will increase from 35% in 2012 to 50% in 2035 [1,2]. This prediction is supported by the rapid progress achieved in recent years in horizontal drilling and hydraulic fracturing technology, which has enhanced technically and economically the exploration of extensive shale formations around North America [3–5]. In fact, the current advances in shale gas production have significantly altered the worldwide energy scenario for any foreseeable future [6,7]. In Europe, shale gas exploration has emerged as an attractive energy source mainly due its supply reliability. Contrarily to petroleum-based energy sources, natural gas production from unconventional reservoirs like shale deposits does not depend of unstable foreign markets that often dictate elevated prices.

Natural gas production from shale formations requires well stimulation for starting and maintaining the process, due to the low gas permeability on the rock [8,9]. Hence, the wells must be drilled and fractured to retrieve the tight gas trapped in the shale rock formations. For this reason, shale gas production consists of an unconventional gas drilling technology that requires large amounts of water for hydraulic fracturing of each well [10]. The fracturing fluids are injected into the horizontal well under high pressure creating a complex artificial fracture network

* Corresponding author.
E-mail addresses: viviani.onishi@ua.es, viviani.onishi@pq.cnpq.br (V.C. Onishi).

http://dx.doi.org/10.1016/j.desal.2016.11.003

to promote gas exhaustion. Usually, six or more wells are drilled horizontally through an extension of up to 2000 m, with a fracture network depth that can reach 500 m into the shale formation [11].

Actually, the development of technologies for drilling and hydro fracturing of shale gas plays are strongly conditioned by the water availability and flowback water disposal [5,12]. Recent studies estimate that the hydraulic fracturing of one single horizontal well demands approximately 3–6 million gallons of water (10,500–21,500 m^3) [13,14]. The hydraulic fracturing fluid is predominantly composed by water and sand (~98%) containing several chemicals such as corrosion inhibitors, surfactants, friction reducers, acids, flow improvers [3]. Approximately 10–80% of the amount of injected fluid flows back to surface during the first two weeks from the beginning of well exploitation [11,15]. Along with the chemical additives utilized for fracturing the wells, flowback water also contains high concentrations of salts and other minerals. Table 1 presents average and maximum values achieved for the flowback water salinity from important U.S. shale plays, expressed in terms of the total dissolved solids (TDS). The flowback water can be recovered for recycling as injection water or for other purposes, demanding specific treatment before any disposal and/or reuse.

Several works have been dedicated to the design and operation of shale gas supply chains for optimal water management [1,4,16–19]. Other studies have focused on the minimization of water consumption [5,13] and gaseous emissions [3,20] during shale gas production. However, available literature about the treatment of high-salinity flowback water is scarce. It is worth noting that the water produced from shale gas drilling and fracturing can represent a serious environmental problem, due to high concentrations of TDS and other pollutants.

The great potential of shale gas production at global scale highlights the need to develop more cost-effective processes for the treatment of the shale gas flowback water. Shaffer et al. [21] have critically reviewed promising technologies for desalination of high-salinity produced water from shale gas exploration. According to the authors, mechanical vapor recompression (MVR) systems are often more advantageous than membrane-based technologies for water desalination [22]. MVR systems require less extensive pretreatment processes because they are usually less susceptible to fouling problems caused by the presence of grease and oil.

There are several publications addressing the optimization problem of multiple-effect evaporation (MEE) systems. The first references in the field date from 1840, with the MEE system being one of the oldest and most widely used water desalination process around the globe [23]. Halil and Söylemez [24] have developed a mathematical modeling approach for the design and simulation of MEE processes for seawater desalination, considering forward feed configuration and renewable energy sources. Gautami and Khanam [25] have proposed nonlinear programming (NLP) models for MEE synthesis and optimization. The optimal design configuration is chosen according to the steam economy in the process. In the work of Druetta et al. [26], a nonlinear mathematical model based on energy and mass balances is presented to predict the optimal MEE performance in terms of energy efficiency. The MEE model is successfully applied to seawater desalination, and the sensitivity analysis and simulations show good accuracy with realistic designs. Posteriorly, the model has been extended in Druetta et al. [27] to determine the equipment capacity and operational conditions by considering the minimization of process costs as the objective function. Al-Mutaz and Wazeer [28] have proposed mathematical models to evaluate the performance of distinct configurations of conventional MEE systems, including forward, backward and parallel/cross feed. More recently, Al-Mutaz [23] has published a comparative study on different seawater desalination plants. His work indicates power consumption efficiency as the main feature for making the MEE process more attractive than the dominant multistage flash (MSF) [29–32] and reverse osmosis (RO) [33–38] desalination processes. Piacentino [39] has introduced an in-depth cost analysis for multiple-effect distillation plants, through the calculation of exergetic efficiency at subcomponent levels. His study introduces some key considerations when developing thermo-economical models.

EI-Dessouky et al. [32,40–44] have made important contributions in mathematical modeling and design of MEE systems with/without mechanical (MVR) or thermal vapor recompression (TVR). In EI-Dessouky et al. [40], different models are presented for MEE systems design including MVR and TVR for seawater desalination. Mathematical models for optimizing single-effect evaporation (SEE) systems with mechanical vapor recompression can be found in several studies in the literature [44–52]. Al-Juwayhel [45] have developed a comprehensive design model for the design of SEE including MVR process. The model has posteriorly been expanded by Ettouney [44] for determining the geometrical characteristics of the evaporator, in addition to the heat transfer area and power consumption calculations. The optimization of SEE systems with MVR using mathematical programming has also been studied by Mussati et al., [53] considering several non-convex constraints. Nevertheless, it should be underlined that all of the above-mentioned works were applied only to seawater desalination. Therefore, in previous studies no considerations have been made about the treatment of very concentrated feed and achievement of zero liquid discharge (ZLD) of brine.

ZLD systems have been studied by Thu et al. [54], by considering an advanced multiple-effect adsorption process. The desalination process is developed to efficiently deal with high-salinity feed water, including brine from other seawater desalination plants. Chung et al. [55] have also investigated ZLD application for the desalination of highly concentrated water by allowing brine discharge close to NaCl saturation conditions. In their work, an approach based on finite differences is used to numerically simulate a multistage membrane distillation process. Although the process can represent an attractive alternative over usual thermal desalination systems due to scale facility, by analyzing exergetic and energetic process efficiencies, the authors have concluded that the required specific membrane area will determine its economic viability.

To surpass the aforementioned limitations, we introduce a new mathematical programming model for optimizing single and multiple-effect evaporation (SEE/MEE) systems, including vapor recompression cycle and thermal integration. The SEE/MEE process is conceived for the treatment of high-salinity flowback water originated during shale gas hydraulic fracturing process. The main objective of the proposed SEE/MEE system is to produce fresh water and concentrated saline close to ZLD, considering the outflow brine salinity near to salt saturation conditions. For this purpose, the multiple-effect superstructure for flowback water desalination includes as many evaporation effects as there are flashing tanks, placed intermittently. As a result, process energy efficiency is further enhanced by recuperating the condensate vapor. The evaporation system is designed with a counter-current flow configuration. Thus, concentrated brine is recovered in the first evaporator effect, while feed water is added to the last one after preheating. In addition, the vapor formed by evaporation and condensate flashing is compressed through multistage electric-driven mechanical equipment

Table 1
Flowback water salinity from different U.S. shale plays expressed in terms of total dissolved solids (TDS).

Report	U.S. Shale play	TDS, ppm	
		Average	Maximum
Acharya et al. [12]	Fayetteville	13 k	20 k
	Woodford	30 k	40 k
	Barnett	80 k	>150 k
	Marcellus	120 k	>280 k
	Haynesville	110 k	>200 k
Hayes [63]			
Haluszczak et al. [15]	Marcellus	157k[a]	228k[a]
Thiel and Lienhard [69]	Marcellus	145 k	–
Jiang et al. [70]	Marcellus	–	261 k

[a] TDS values for the flowback water in 14th day of hydraulic fracturing.

containing intercoolers. Consequently, the SEE/MEE process does not require any other external energy source.

The superstructure is mathematically formulated as an NLP model solved using GAMS, minimizing the total annualized cost of the process. The SEE and MEE optimal configurations including vapor recompression cycle and heat integration are compared in terms of their ability to achieve ZLD conditions for the brine concentrate. Sensitivity analysis is performed to assess the optimal evaporation process configuration and performance under different flowback water salinities. In addition, the obtained results are validated by simulations using Aspen HYSYS software.

The main novelties introduced by this work include: (*i*) development of a more comprehensive and robust NLP model for the optimal simultaneous synthesis of SEE/MEE systems, including vapor recompression cycle and thermal integration; (*ii*) application of the proposed SEE/MEE model to the treatment of high-salinity flowback water, originating from the hydraulic fracturing process in shale gas production; (*iii*) SEE/MEE model application to ZLD conditions of the concentrated brine and the high recovery ratio of fresh water; (*iv*) capability of the SEE/MEE model to effectively deal with very high concentrations of the feed water; and, (*v*) facility of process scaling.

This paper is structured as follows: Section 2 presents the formal problem statement, wherein the study boundaries are defined and the major process features are described in detail. In Section 3, we develop the mathematical NLP model for the simultaneous SEE/MEE synthesis. The capabilities of our developed SEE/MEE model are evaluated in Section 4, by applying it to a case study based on shale gas production. In addition, this section shows the main results and discussions about the sensitivity analysis and HYSYS simulations, and the most important computational aspects. Finally, the conclusions of the work are presented in Section 5.

2. Problem statement

Given is a high-salinity flowback water stream from shale gas production, with a known supply state (inlet mass flowrate, salinity, temperature and pressure) and target specification defined by the brine concentration. Additionally, equipment (for promoting heat exchange, evaporation, compression and separation) and energy services (including cooling water and electric power) are also provided, with their respective costs. The goal is to identify the optimal SEE/MEE system configuration, considering the vapor recompression cycle and thermal integration, by minimizing the process total annualized cost. The optimal process configuration should achieve a high recovery ratio of fresh water produced and brine close to the ZLD condition. The objective function is composed of the capital cost of investment in equipment and the operating expenses related to cold utility and electricity.

It should be highlighted that improving the process cost-effectiveness through the reduction of brine discharges (*i.e.*, achieving ZLD conditions and consequently, increasing the fresh water production), allows lessening the environmental impacts associated to energy consumption and waste disposal. Shale gas exploration is a recent technology that requires further development, particularly in the framework of the flowback water treatment. To the best of our knowledge, this is the first work proposing the ZLD application to the treatment of the flowback water from shale gas fracking, through a SEE/MEE system including MVR and thermal integration. The multiple-effect superstructure proposed for the desalination of shale gas flowback water is showed in Fig. 1.

The following equipment are considered in the MEE system with vapor recompression and thermal integration:

(i) Shell-and-tube preheater (for the heat exchange between feed water and condensate).
(ii) Multiple-effect evaporator.
(iii) Multistage electricity-driven compressor with intercoolers.
(iv) Flashing tanks.
(v) Pumps and mixers.

The MEE system comprises *i* evaporation effects intermediately coupled to flashing tanks that are used to recover condensate vapor, enhancing process energy efficiency. Note that the SEE system corresponds to a simplification of the MEE process, being composed of a single-effect evaporator without a flash tank. In this case, vapor flashing is not allowed due to the low amount of recoverable energy from the condensate, which makes unfeasible the capital cost related to the allocation of such equipment.

In the proposed MEE system, the evaporation effects are numbered according to the direction of the heat flow (*i.e.*, from 1 to *i*). The evaporator effect *i* is composed of the shell containing droplet separator (to remove water from the saturated vapor), spaces for the saturated vapor and saline pool, brine spray nozzles and evaporation/condensation tubes. A counter-current flow configuration is considered such that the vapor from the last evaporation effect and the condensate vapor from the last flash tank are compressed, through a mechanical equipment composed by *j* stages. Thus, the superheated compressed vapor is added in the first evaporation effect, whereas the feed water (corresponding to the shale gas flowback water) is inserted in the last one. It should be noted that the vapor recompression process is cyclic. Thus, the entire amount of vapor formed in the last evaporator effect is routed to the mechanical vapor compressor together with the flashed off condensate vapor from last flash tank —to be superheated to a desired target condition— before being added to the first evaporation effect. It should be emphasized that the vapor recompression cycle allows further enhancing heat integration in evaporation systems, because it operates on all the vapor originated from the evaporation system, providing the energy required in the process [56].

Under this system configuration, the first evaporation effect should present the highest temperature and pressure, while the last effect *i* should be subjected to the lowest conditions for these variables. Moreover, the vapor formed in the system follows the direction of dropping pressure (and temperature). The brine (feed) flows in the opposite direction. The superheated vapor from compression (for effect 1), as well as the vapor formed in previous effects (for effects 2 to *i*), are introduced inside the evaporator tubes. The feed water (*i.e.*, brine from subsequent stages for effects 1 to *i*-1; and, shale gas flowback water in effect *i*) is sprayed on the tubes in the shell-side to promote evaporation. In this way, the vapor is condensed on the tube-side by transferring its latent heat to the falling film formed by the sprayed feed. Observe that in the first effect, the formed falling film outside tubes absorbs the latent heat from the compressed vapor starting the process of feed (*i.e.*, brine from effect 2) evaporation. The vapor formed is used to drive effect 2. This process occurs successively until last effect *i*. Still in effect 1, sensible heat is responsible for the temperature change in the tube-side, wherein the condensed vapor changes from the inlet superheated vapor temperature to its desired outlet condition. Note that the condensate outlet temperature should correspond to the inlet vapor saturation pressure.

After each evaporation effect, the condensed vapor is sent to flash tanks to reduce its pressure (and temperature) and, consequently, recover energy. The small amount of flashed off condensate vapor in an effect *i*, plus the vapor formed by boiling in the previous effect are added to the tube-side of the subsequent evaporation effect. For this reason, both streams should be at the same pressure. Before entering into the evaporator, the feed water is preheated taking in advantage the sensible heat from the condensed vapor (*i.e.*, produced fresh water) to improve heat integration in the evaporation system [57]. The increase in the feed temperature is essential for improving the energy recovery and maintaining the system productivity in the presence of climatic changes throughout the year.

The SEE/MEE synthesis with MVR and thermal integration is a complex process and we seek the optimal system configuration

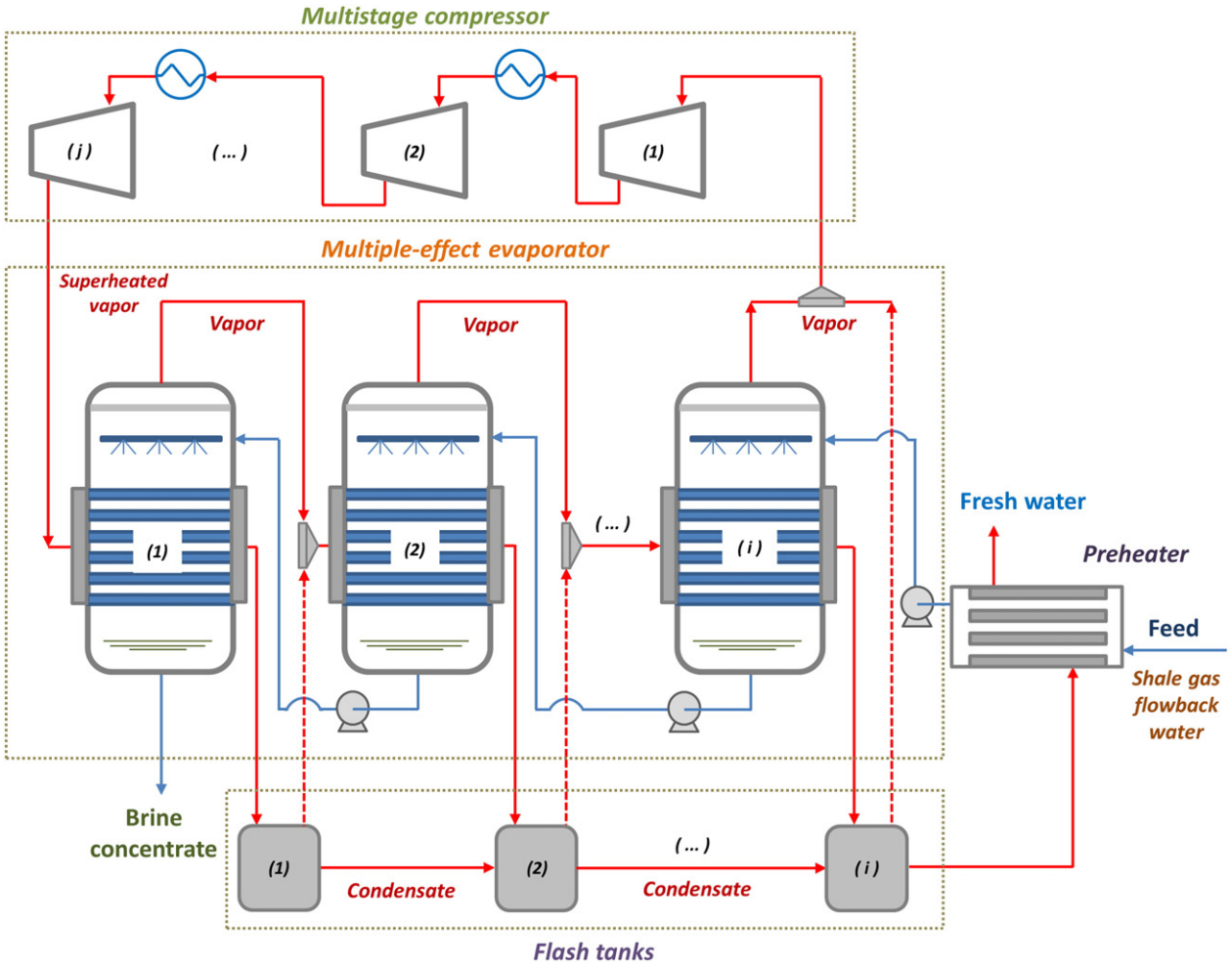

Fig. 1. Multiple-effect evaporation superstructure proposed for the desalination of high-salinity flowback water from shale gas fracking.

corresponding to lower heat transfer area and minimum services consumption (including thermal utilities and electricity). For this purpose, all flows properties (*i.e.*, temperature, pressure, specific enthalpy, concentration and flowrate) are unknown variables needing optimization. Fig. 2 (*a*) shows the main process variables for the effect *i* of the evaporator and flash tank *i*, while Fig. 2 (*b*) displays the system variables for the stage *j* of compression. Moreover, the elevated number of temperature constraints to guarantee the optimal equipment functioning, allied to the high non-convexity and nonlinearity of the cost correlations further increase the complexity of the model.

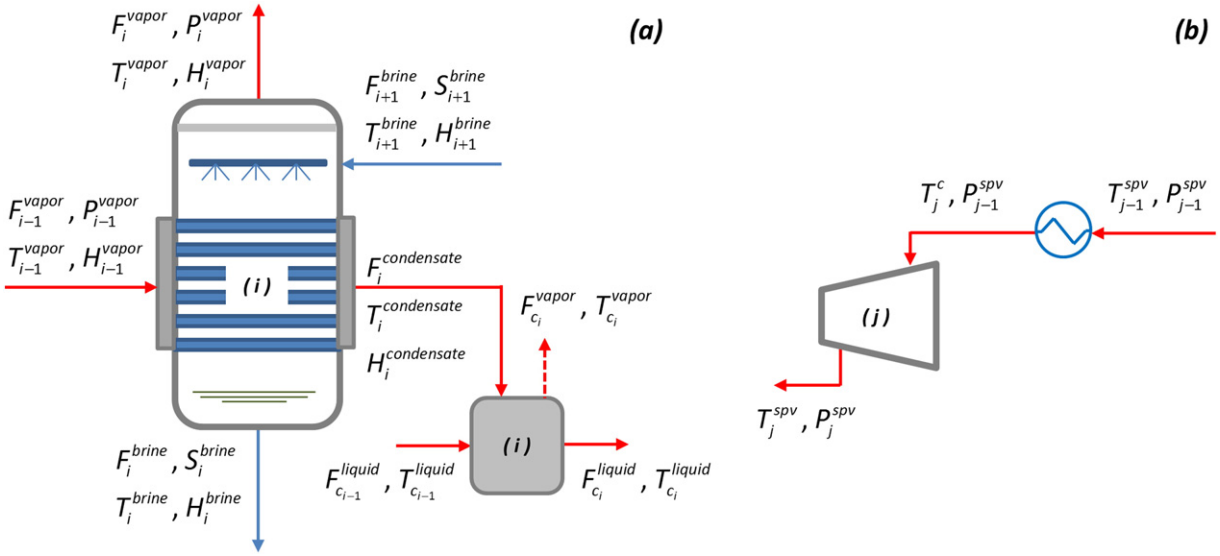

Fig. 2. Process decision variables for (*a*) the effect *i* of the evaporator and flash tank *i*; and, (*b*) the stage *j* of the compressor.

For the desalination of the shale gas flowback water, it is assumed that the feed water has been previously treated to remove all contaminants, including chemical additives (such as flow improvers, acids, surfactants, friction reducers, and corrosion inhibitors), oils, greases and sand. Water pretreatment technologies can include filtration, chemical and physical precipitation, sedimentation and flotation. However, the shale gas flowback water still has high TDS concentration after pretreatment. The objective of the proposed SEE/MEE system is to supply, in combination with suitable water pretreatment technologies, high cost-effective recovery of fresh water for reuse or for safe disposal. Also, the system should operate at low pressure and temperature to prevent equipment instability and avoid corrosion and fouling problems, which can be caused by the high salt concentration and the presence of remaining oils and greases. In addition, the lower operation temperatures allow for reducing process scaling and thermodynamic losses, allowing for minimal thermal insulation [41,43].

Due to the use of an electric-driven mechanical compressor, the SEE/MEE system does not require an external energy source. An energy generator can be used when electricity services are not available, making the SEE/MEE process suitable for use in remote off-grid locations. Other advantages of the SEE/MEE system include the consideration of horizontal tube configuration, in which the falling film formed allows for higher heat transfer coefficients and lower heat transfer areas [58]. This reduces the capital costs of investment and equipment size, making the process more compact and therefore more easily transported. Moreover, the MEE system permits the simple inclusion of additional evaporation effects due to its modular feature.

The following assumptions are considered to simplify the mathematical formulation:

(vi) Steady state operation.
(vii) Heat losses in all thermal and mechanical equipment are neglected.
(viii) The non-equilibrium allowance (NEA) is neglected.
(ix) Pressure drops in all thermal and mechanical equipment are neglected.
(x) Zero salinity for the condensate (product).
(xi) Vapor streams from each evaporator effect behave as ideal gases.
(xii) All effects of the evaporator are built with nickel (to avoid corrosion).
(xiii) The multi-stage compressor is centrifugal (without drivers) built with carbon steel.
(xiv) Starter energy required for the multi-stage compressor is neglected.
(xv) Effect of surging and choking is disregarded in the multi-stage compressor.
(xvi) The vapor multi-stage compression is isentropic.
(xvii) Shell-and-tube preheater and flash tanks are built with carbon steel.
(xviii) Capital costs of pumps and mixers are negligible.

The mathematical formulation of the proposed model including equality and inequality constraints for the optimal SEE/MEE process synthesis is presented in the following section.

3. Mathematical programming model

The mathematical programming model for optimizing SEE/MEE systems is formulated based on the superstructure presented in Fig. 1. The proposed superstructure is composed by i evaporation effects coupled intermediately to i flashing tanks, and j compression stages. The inlet temperature ($T_{in}^{feed\_water}$), mass flowrate ($F_{in}^{feed\_water}$) and salt concentration ($S_{in}^{feed\_water}$) of the feed water (*i.e.*, shale gas flowback water) are known parameters for the model. The outlet conditions of the produced fresh water—including temperature ($T_{out}^{fresh\_water}$) and flowrate ($F_{out}^{fresh\_water}$)—are variables that must be optimized by considering brine salinity specifications (S_{out}^{brine}). All intermediate streams temperatures (T), pressures (P), specific enthalpies (H), salt concentrations (S) and mass flowrates (F), as well as the system performance characteristics (including compression work W, heat transfer area A and heat flow Q) are decision variables requiring optimization. The mathematical model formulation comprises mass and energy balances on all equipment and mixing points, and design constraints involving stream temperatures and pressures to avoid solutions without physical meaning. The objective function accounts for the total annualized process cost, which is composed by operational expenses and capital investment. The resulting NLP-based model is developed in the next sections, in which the SEE/MEE superstructure is generated according to the following steps.

3.1. Sets definition

The following sets are required to develop the NLP model.

$I = \{i/i \text{ is an evaporator effect}\}$
$J = \{j/j \text{ is a compression stage}\}$

Note that the number of evaporation effects and compression stages can be chosen arbitrarily. However, the selection of larger values for these indices will increases the problem size and complexity and, consequently, the difficulty in obtaining a solution.

3.2. Multiple-effect evaporator

The multiple-effect evaporator design is as follows.

3.2.1. Evaporator mass balances

For effects 1 to i-1, the feed water corresponds to the brine from subsequent effects at F_{i+1}^{brine} and S_{i+1}^{brine} conditions. In the last effect i, the feed stream is the shale gas flowback water to be treated (under $F_i^{feed\_water}$ and $S_{in}^{feed\_water}$ conditions). Thus, the mass balances for the effect i-1 of the multiple-effect evaporator are given by:

$$F_{i+1}^{brine} = F_i^{brine} + F_i^{vapor} \quad 1 \le i \le I-1 \tag{1}$$

$$F_{i+1}^{brine} \cdot S_{i+1}^{brine} = F_i^{brine} \cdot S_i^{brine} \quad 1 \le i \le I-1 \tag{2}$$

Observe that for the first effect, the salinity of the brine should correspond to its outlet specification S_{out}^{brine}. In this study, we consider the brine outlet specification near to salt saturation concentration to achieve zero liquid discharge conditions. For the last evaporation effect, the mass and salt balances are:

$$F_i^{feed\_water} = F_i^{brine} + F_i^{vapor} \quad i = I \tag{3}$$

$$F_i^{feed\_water} \cdot S_{in}^{feed\_water} = F_i^{brine} \cdot S_i^{brine} \quad i = I \tag{4}$$

3.2.2. Ideal temperature

The ideal temperature T_i^{ideal} is defined as the temperature that an effect i should have if its brine salinity is equal to zero. The ideal temperature in effect i is estimated by Eq. (5).

$$\ln\left(P_i^{vapor}\right) = a + b/\left(T_i^{ideal} + c\right) \quad \forall i \in I \tag{5}$$

The values for the Antoine parameters a, b and c in the Eq. (5) are 12.98437, −2001.77468 and 139.61335, respectively. These correlation parameters have been obtained from HYSYS-OLI process simulator by considering the temperature in a range of $10 \le T_i \le 120$°C and salt mass

fractions XS_i^{brine} between 0 and 0.3, under the electrolytes thermodynamic package.

3.2.3. Boiling point elevation (BPE)

The boiling point elevation (BPE) corresponds to the increase in the boiling point temperature caused by the brine salt concentration. The BPE is calculated as a function of the salt mass fraction (XS_i^{brine}) and the ideal temperature (T_i^{ideal}) in an evaporation effect *i*.

$$BPE_i = 0.1581 + 2.769 \cdot XS_i^{brine} - 0.002676 \cdot T_i^{ideal} + 41.78\left(XS_i^{brine}\right)^{1/2} + 0.134 \cdot XS_i^{brine} \cdot T_i^{ideal} \quad (6)$$

In which,

$$XS_i^{brine} = 0.001 \cdot S_i^{brine} \quad \forall i \in I \quad (7)$$

3.2.4. Brine temperature

The brine temperature (T_i^{brine}) in an evaporation effect *i* should be equal to its BPE added to its ideal temperature (T_i^{ideal}). In fact, the brine temperature is considered to be the effect temperature. Thus, the brine and outlet vapor in an effect *i* (T_i^{vapor}) should be at the same temperature T_i^{brine}.

$$T_i^{brine} = T_i^{ideal} + BPE_i \quad \forall i \in I \quad (8)$$

3.2.5. Evaporator energy balances

The overall energy balance for effect *i* should include the heat flows added to the system boundary from feed water and condensed vapor, and the vapor and brine energy outflows. The overall energy balances in each effect of the evaporator is given by Eq. (9) and Eq. (10).

$$Q_i^{evaporator} + F_{i+1}^{brine} \cdot H_{i+1}^{brine} = F_i^{brine} \cdot H_i^{brine} + F_i^{vapor} \cdot H_i^{vapor} \quad i<I \quad (9)$$

$$Q_i^{evaporator} + F_i^{feed\_water} \cdot H_i^{feed\_water} = F_i^{brine} \cdot H_i^{brine} + F_i^{vapor} \cdot H_i^{vapor} \quad i = I \quad (10)$$

For which the specific enthalpies of the vapor, brine and feed water (*i.e.*, shale gas flowback water) streams are estimated by the following correlations:

$$H_i^{vapor} = -13470 + 1.840 \cdot T_i^{brine} \quad \forall i \in I \quad (11)$$

$$H_i^{brine} = -15940 + 8787 \cdot XS_i^{brine} + 3.557 \cdot T_i^{brine} \quad \forall i \in I \quad (12)$$

$$H_i^{feed\_water} = -15940 + 8787 \cdot XS_i^{feed\_water} + 3.557 \cdot T_i^{feed\_water} \quad i = I \quad (13)$$

As mentioned before, the vapor and brine streams are at the same temperature T_i^{brine} in effect *i*. However, the specific enthalpy estimation for the brine and for feed water in the last effect should also consider the influence of their salinity in addition to the temperature.

3.2.6. Heat requirements in the evaporator

In the first evaporation effect, the term $Q_i^{evaporator}$ in the Eq. (9) comprises the latent heat needed to condense the superheated vapor from the compressor, and the sensible heat required to achieve the target condensate temperature ($T_i^{condensate}$).

$$Q_i^{evaporator} = F_i^{spv} \cdot Cp^{vapor} \cdot \left(T_j^{spv} - T_i^{condensate}\right) + F_i^{spv} \cdot \left(H_i^{cv} - H_i^{condensate}\right) \quad i = 1, j = J \quad (14)$$

In Eq. (14), Cp^{vapor} is the specific heat for the vapor stream. In this work, it is considered to be constant in order to simplify the model. T_i^{spv} and $T_i^{condensate}$ are the superheated vapor and condensate temperatures, respectively. The condensate temperature $T_i^{condensate}$ is estimated by considering the outlet compressor pressure P_j^{spv} in Antoine equation given by Eq. (5). Moreover, H_i^{cv} and $H_i^{condensate}$ are the specific enthalpies for the vapor and liquid phases of the condensate, respectively. These variables are estimated by Eq. (11) and Eq. (12), considering the outlet condensate temperature $T_i^{condensate}$. Note that the salt mass fraction in Eq. (12) should be equal to zero for the liquid specific enthalpy estimation. The variable F_i^{spv} indicates the superheated vapor flowrate, which includes the vapor flowrates from the last evaporator effect and flashing tank:

$$F_1^{spv} = F_i^{vapor} + F_{c_i}^{vapor} \quad i = I \quad (15)$$

For effects 2 to *i*, the heat requirements include the contributions of the vaporization latent heat added by the boiling vapor, and the flashed off condensate vapor from previous effect. The heat flows in each evaporation effect are given by the following equation.

$$Q_i^{evaporator} = F_{i-1}^{vapor} \cdot \lambda_i + F_{c_{i-1}}^{vapor} \cdot \lambda_i \quad i>1 \quad (16)$$

In Eq. (16), F_{i-1}^{vapor} and $F_{c_{i-1}}{}^{vapor}$ are the boiling vapor and flashed off condensate vapor flowrates from the previous effect, respectively. The latent heat of vaporization λ_i is calculated by the following correlation:

$$\lambda_i = 2502.5 - 2.3648 \cdot T_i^{sv} + 1.840\left(T_{i-1}^{sv} - T_i^{sv}\right) \quad i>1 \quad (17)$$

In which T_i^{sv} is the saturated vapor temperature estimated by Eq. (5) corresponding to the saturated vapor pressure P_i^{sv}.

3.2.7. Feasibility of pressure and temperature between evaporator effects

The outlet vapor pressure throughout the different effects of the evaporator should decrease monotonically. Moreover, the outlet vapor pressure P_i^{vapor} in effect *i* should be equal to the saturated vapor pressure from the following effect $i + 1$ to avoid instabilities in the equipment.

$$P_i^{vapor} \geq P_{i+1}^{vapor} + \Delta P_{\min} \quad i<I \quad (18)$$

$$P_i^{vapor} = P_{i+1}^{sv} \quad i<I \quad (19)$$

3.2.8. Overall heat transfer coefficient. The overall heat transfer coefficient $U_i^{evaporator}$ is estimated using the correlation presented by Al-Mutaz and Wazeer [28].

$$U_i^{evaporator} = 0.001 \cdot \left(1939.4 + 1.40562 \cdot T_i^{brine} - 0.00207525 \cdot \left(T_i^{brine}\right)^2 + 0.0023186 \cdot \left(T_i^{brine}\right)^3\right) \quad (20)$$

3.2.9. Evaporator heat transfer area. The evaporator is designed to be a compact piece of equipment composed of several evaporation effects. For this reason, a total heat transfer area should be determined for estimating costs. The total heat transfer area of the evaporator effects ($A_{T}{}^{evaporator}$) is given by Eq. (21).

$$A^{evaporator} = \sum_{i=1}^{I} A_i = \sum_{i=1}^{I} Q_i / (U_i \cdot LMTD_i) \quad (21)$$

In the first effect of the evaporator, the heat transfer area should be equal to the sum of the sensible and latent heat transfer areas. For the calculation of the transfer area for sensible heat, the overall heat transfer

coefficient U^S is considered as a known parameter.

$$A_i = A_i^1 + A_i^2 \quad i = 1 \tag{22}$$

$$A_i^1 = F_i^{spv} \cdot Cp^{vapor} \cdot \left(T_j^{spv} - T_i^{condensate}\right) / \left(U^S \cdot LMTD_i\right) \quad i = 1, j = J \tag{23}$$

$$A_i^2 = F_i^{spv} \cdot \left(H_i^{cv} - H_i^{condensate}\right) / U_i \cdot \left(T_i^{condensate} - T_i^{brine}\right) \quad i = 1 \tag{24}$$

In order to avoid numerical difficulties related to matching temperature differences, Chen's approximation [59] is used to determine the logarithmic mean temperature difference ($LMTD_i$).

$$LMTD_i = \left(0.5 \cdot (\theta_{1i} \cdot \theta_{2i})(\theta_{1i} + \theta_{2i})\right)^{1/3} \quad i \in I \tag{25}$$

In which,

$$\theta_{1i} = \begin{cases} T_j^{spv} - T_i^{brine} & i = 1, j = J \\ T_i^{sv} - T_i^{brine} & i > 1 \end{cases} \text{ and } \theta_{2i} = \begin{cases} T_i^{condensate} - T_{i+1}^{brine} & i = 1 \\ T_i^{sv} - T_{i+1}^{brine} & 1 < i < I \\ T_i^{sv} - T_i^{feed} & i = I \end{cases} \tag{26}$$

For obtaining a more uniform area distribution, the following restrictions are considered:

$$A_i \leq n \cdot A_{i-1} \quad i > 1 \tag{27}$$

$$A_i \geq A_{i-1} \quad i > 1 \tag{28}$$

In which n is set to be equal to 3. However, it should be noted that the parameter n can be chosen arbitrarily according to the designer need. If necessary, the constraint can be easily removed from the model.

3.2.10. Temperature constraints

Constraints on temperature must be used to avoid temperature crossovers in the evaporator effects. These constraints are defined by the Eqs. (29)–(36).

$$T_j^{spv} \geq T_i^{condensate} + \Delta T_{\min}^1 \quad i = 1, j = J \tag{29}$$

$$T_{i-1}^{brine} \geq T_i^{condensate} + \Delta T_{\min}^1 \quad i > 1 \tag{30}$$

$$T_i^{brine} \geq T_{i+1}^{brine} + \Delta T_{\min}^{stage} \quad i < I \tag{31}$$

$$T_i^{brine} \geq T_i^{feed} + \Delta T_{\min}^2 \quad i = I \tag{32}$$

$$T_i^{condensate} \geq T_{i+1}^{brine} + \Delta T_{\min} \quad i < I \tag{33}$$

$$T_i^{condensate} \geq T_i^{feed} + \Delta T_{\min} \quad i = I \tag{34}$$

$$T_i^{condensate} \geq T_i^{brine} + \Delta T_{\min} \quad i \in I \tag{35}$$

$$T_i^{sv} \geq T_i^{brine} + \Delta T_{\min} \quad i \in I \tag{36}$$

3.3. Condensate flashing tanks

The condensate flashing tanks are modeled using the following equations.

3.3.1. Mass balances in the flashing tank i

The mass balances in each flash tank i are given by the equations:

$$F_i^{spv} = F_{c_i}^{vapor} + F_{c_i}^{liquid} \quad i = 1 \tag{37}$$

$$F_{i-1}^{vapor} + F_{c_{i-1}}^{vapor} + F_{c_{i-1}}^{liquid} = F_{c_i}^{vapor} + F_{c_i}^{liquid} \quad i > 1 \tag{38}$$

In which $F_{c_i}^{vapor}$ and $F_{c_i}^{liquid}$ are the mass flowrates for the flashed off vapor and liquid phases of the condensate, respectively.

3.3.2. Energy balances in the flashing tank i

The energy balances in each flash tank i are given by the equations:

$$F_i^{spv} \cdot H_i^{condensate} = F_{c_i}^{vapor} \cdot H_{c_i}^{vapor} + F_{c_i}^{liquid} \cdot H_{c_i}^{liquid} \quad i = 1 \tag{39}$$

$$\left(F_{i-1}^{vapor} + F_{c_{i-1}}^{vapor}\right) \cdot H_i^{condensate} + F_{c_{i-1}}^{liquid} \cdot H_{c_{i-1}}^{liquid} = F_{c_i}^{vapor} \cdot H_{c_i}^{vapor} + F_{c_i}^{liquid} \cdot H_{c_i}^{liquid} \quad i > 1 \tag{40}$$

In which $H_i^{condensate}$ and $H_{c_i}^{liquid}$ are the liquid specific enthalpies estimated by the Eq. (12) considering the temperatures of condensate $T_{condensate}^{r}$ and ideal T_i^{ideal}, respectively. In both cases, salt mass fraction equal to zero (*i.e.*, $XS_i^{brine} = 0$) is assumed in Eq. (12). The specific enthalpy for the flash off vapor $H_{c_i}^{vapor}$ from the condensate is obtained by Eq. (11), considering the ideal temperature in the effect.

3.3.3. Volume of the flashing tank i

The volume of each flashing tank i is given by the following equations:

$$V_i^{flash} = \left(F_i^{spv} \cdot t\right) / \rho \quad i = 1 \tag{41}$$

$$V_i^{flash} = \left(F_{i-1}^{vapor} + F_{c_{i-1}}^{liquid}\right) \cdot t / \rho \quad i > 1 \tag{42}$$

In which t indicates the retention time of the condensate inside the flash tank, and ρ the water density. In this study, a retention time equal to 5 min is considered for flashing tanks design.

3.4. Condensate/feed preheater

The condensate/feed preheater used to heat the feed water is designed using the following equations.

3.4.1. Energy balance in the condensate/feed preheater

The energy balance in the preheater is given by Eq. (43).

$$F_{c_i}^{liquid} \cdot Cp_i^{condensate} \cdot \left(T_i^{ideal} - T_{out}^{fresh\_water}\right) = F_{in}^{feed\_water} \cdot Cp_{in}^{feed} \cdot \left(T_i^{feed\_water} - T_{in}^{feed}\right) \quad i = I \tag{43}$$

In which T_{in}^{feed} is the inlet feed temperature of the shale gas flowback water. $Cp_i^{condensate}$ and Cp_{in}^{feed} are the specific heats of the condensate (*i.e.*, fresh water produced) and feed water, respectively. The liquid specific heats are estimated by the following correlations:

$$Cp_{in}^{feed} = 0.001 \cdot \left[\begin{array}{l} \left(4206.8 - 6.6197 \cdot S_{in}^{feed\_water} + 1.2288e^{-2} \cdot \left(S_{in}^{feed\_water}\right)^2\right) + \\ \left(-1.1262 + 5.418e^{-2} \cdot S_{in}^{feed\_water}\right) \cdot T_{in}^{feed} \end{array}\right] \quad i = I \tag{44}$$

$$Cp_i^{condensate} = 0.001 \cdot \left(4206.8 - 1.1262 \cdot T_i^{ideal}\right) \quad i = I \tag{45}$$

3.4.2. Heat transfer area of the condensate/feed preheater

The heat transfer area $A^{preheater}$ of the condensate/feed preheater is determined by the equation:

$$A^{preheater} = F_{c_i}^{liquid} \cdot Cp_i^{condensate} \cdot \left(T_i^{ideal} - T_{out}^{fresh\_water}\right) / U^{preheater} \cdot LMTD^{preheater} \quad i = I \tag{46}$$

In which, the overall heat transfer coefficient $U^{preheater}$ is estimated by Eq. (20) considering the ideal temperature T_i^{ideal} for the last evaporator effect. In this case, the log mean temperature difference ($LMTD^{preheater}$) is calculated by Eq. (25), with the temperature difference in the hot and cold terminals given by:

$$\theta_1^{preheater} = T_i^{ideal} - T_i^{feed\_water} \quad i = I \quad \text{and} \quad \theta_2^{preheater} = T_{out}^{fresh\_water} - T_{in}^{feed} \tag{47}$$

3.5. Multistage mechanical compressor

The multistage mechanical compressor with intercooling is designed using the following mathematical formulation.

3.5.1. Heat duty

The amount of heat Q_j^{cooler} exchanged by the intercooler is given by Eq. (48).

$$Q_j^{cooler} = F_i^{spv} \cdot Cp^{vapor} \cdot \left(T_{j-1}^{spv} - T_j^c\right) \quad j>1 \tag{48}$$

In which T_{j-1}^{spv} is the inlet temperature in the intercooler that should correspond to the compressor outlet temperature from the previous stage. On the other hand, T_j^c is the intercooler outlet temperature, which should be equal to the inlet temperature in the next compression stage.

3.5.2. Constraints on intercoolers temperatures

Constraints are necessary to ensure that the outlet temperature from an intercooler is lower than the correspondent inlet temperature on it (*i.e.*, the vapor stream should be cooled):

$$T_{j-1}^{spv} \geq T_j^c + \Delta T_{\min}^{cooler} \quad j>1 \tag{49}$$

Note that the outlet intercooler temperature should be above the saturation temperature in order to avoid the presence of liquid in the compressor, and related operational issues.

3.5.3. Energy balance in the mixer

An energy balance is needed in the mixer allocated before the compressor, to guarantee that the inlet vapor temperature in such equipment is at mixture temperature T_i^m.

$$F_{c_i}^{vapor}\left(T_i^m - T_i^{ideal}\right) = F_i^{vapor} \cdot \left(T_i^{brine} - T_i^m\right) \quad i = I \tag{50}$$

3.5.4. Isentropic temperature

The isentropic temperature of the compressed/superheated vapor is given by the equations:

$$T_j^{is} = (T_i^m + 273.15) \cdot \left(P_j^{spv}/P_i^{vapor}\right)^{(\gamma-1)/\gamma} - 273.15 \quad i = I, j = 1 \tag{51}$$

$$T_j^{is} = \left(T_j^c + 273.15\right) \cdot \left(P_j^{spv}/P_{j-1}^{spv}\right)^{(\gamma-1)/\gamma} - 273.15 \quad j>1 \tag{52}$$

In which γ is the heat capacity ratio. The outlet pressure of the superheated vapor P_j^{spv} in the stage j should be limited to a maximum compression ratio:

$$P_j^{spv} \leq CR_{\max} \cdot P_i^{vapor} \quad i = I, j = 1 \text{ and } P_j^{spv} \leq CR_{\max} \cdot P_{j-1}^{spv} \quad j>1 \tag{53}$$

3.5.5. Temperature of the superheated vapor

The superheated vapor temperature, *i.e.* the compressor outlet temperature in the stage j is calculated by the equation:

$$T_j^{spv} = T_j^c + 1/\eta \cdot \left(T_j^{is} - T_j^c\right) \quad \forall j \in J \tag{54}$$

In which η is the isentropic efficiency of the compressor.

3.5.6. Constraints on compressor temperatures and pressures

In the compression stage j, an increase of the vapor temperature and pressure is expected:

$$T_j^{spv} \geq T_j^c \quad \forall j \in J \tag{55}$$

$$P_j^{spv} \geq P_i^{vapor} \quad i = I, j = 1 \tag{56}$$

$$P_j^{spv} \geq P_{j-1}^{spv} \quad j>1 \tag{57}$$

3.5.7. Compression work

The total compression work is expressed in terms of the enthalpies difference of the compressed superheated vapor H_j^{spv} and the inlet compressor vapor H_j^c in each stage j:

$$W = \sum_{j=1}^{J} W_j = \sum_{j=1}^{J} F_i^{spv} \cdot \left(H_j^{spv} - H_j^c\right) \quad i = 1 \tag{58}$$

In which H_j^{spv} and H_j^c are the specific enthalpies for the vapor streams estimated by Eq. (11), considering the inlet (T_j^c) and outlet (T_j^{spv}) compressor temperatures, respectively. For allowing a more uniform compression capacities distribution, the following restrictions are considered:

$$W_j \leq m \cdot W_{j-1} \quad j>1 \tag{59}$$

$$W_j \geq W_{j-1} \quad j>1 \tag{60}$$

In which m is set to be equal to 3. The parameter m can be chosen arbitrarily according to the designer specification. Note that the equipment is more expensive as higher uniformity is required for the compressor construction. If necessary, the constraint can be easily removed from the model.

3.6. Design specification

To achieve the ZLD condition, the brine salinity at first effect should be at least equal to its design specification.

$$S_i^{brine} \geq S_{out}^{brine} \quad i = 1 \tag{61}$$

All correlations presented in the mathematical formulation —including the correlations for estimation of the BPE (Eq. (6)), liquid and vapor specific enthalpies (Eq. (11)–(13)), latent heat of vaporization (Eq. (17)); and, liquid specific heat (Eq. (44) and Eq. (45)) — have been obtained from HYSYS-OLI simulator by using the thermodynamic package for electrolytes, and considering salt mass fractions between 0 and 0.30.

3.7. Objective function

The objective function corresponds to the minimization of the total annualized cost of the SEE/MEE process with mechanical vapor recompression and heat recovery. The objective function is defined by the following mathematical formulation.

3.7.1. Total annualized cost

The total annualized cost of the SEE/MEE system with mechanical vapor recompression and thermal integration should be equal to the sum between capital costs (*CAPEX*) and operational expenses (*OPEX*) as described by Eq. (62).

$$TAC = CAPEX + OPEX \tag{62}$$

3.7.2. Total capital expenditures

The total capital costs *CAPEX* should account for the investment cost of all equipment in the SEE/MEE system with mechanical vapor recompression and thermal integration. Therefore, the calculation of the total capital cost includes the expenditures for the preheater, multiple-effect evaporator, multistage compressor and flashing tanks.

$$CAPEX = fac \cdot \left(\frac{CEPCI_{2015}}{CEPCI_{2003}}\right) \cdot \left(\begin{array}{l} CPO^{evap} \cdot FBM^{evap} \cdot FP^{evap} + CPO^{comp} \cdot FBM^{comp} \cdot FP^{comp} + \\ \sum_{i=1}^{I} CPO_i^{flash} \cdot FBM^{flash} \cdot FP^{flash} + CPO^{preh} \cdot FBM^{preh} \cdot FP^{preh} \end{array}\right) \tag{63}$$

In which *fac* is the annualization factor for the capital cost as defined by Smith [60]:

$$fac = \frac{r(1+r)^y}{(1+r)^y - 1} \tag{64}$$

In which r is the fractional interest rate per year and y is the number of years (amortization period). In Eq. (63), *CPO* indicates the basic cost of a unitary equipment (in kUS$) operating at pressure close to ambient conditions. *CPO* is estimated using the correlations presented by Turton et al. [61] for the preheater and flashing tanks. For the cost estimation of the evaporator and the multistage compressor, the correlations proposed by Couper et al. [62] are considered. *FBM* corresponds to the factor of correction for the basic unitary cost, in which the construction materials and the operational pressure of these equipment units are correlated. Moreover, the total annualized cost must be corrected for the relevant year using the CEPCI index (Chemical Engineering Plant Cost Index).

3.7.3. Operational expenditures

Operational expenditures comprise the electricity and cooling services consumed by the multistage compressor:

$$OPEX = Ec \cdot \sum_{j=1}^{J} W_j + Cc \cdot \sum_{j=1}^{J} Q_j^{cooler} \tag{65}$$

In which *Ec* and *Cc* are the cost parameters for electricity and cooling services, respectively.

4. Case study

A case study is performed to verify the accuracy of the proposed mathematical model for optimizing SEE/MEE systems, considering vapor recompression cycle and thermal integration. It should be highlighted that the problem data used in this example are based on real data obtained from important U.S. shale plays such as Marcellus and Barnett [63–66]. The capacity of the centralized treatment plant should be 900 $m^3\ day^{-1}$ (or 10.42 kg s^{-1}) of shale gas flowback water. Interestingly, Lira-Barragán et al. [4] report in a recent work that under an uncertain scenario as the amount of water required to complete each well (*i.e.*, considering a standard deviation of 10% in the shale plays data), the choice of the aforementioned value (900 $m^3\ day^{-1}$) has 100% probability of guaranteeing that the plant capacity is adequate to treat the total amount of flowback water. These authors have considered a mean value of 15 k m^3 (in a range of 12–18 k m^3) for the amount of water needed for the hydraulic fracturing of each well, from which 25% is expected to return to surface as flowback water during the first 3 weeks. Additionally, the total number of wells to be treated is divided in fracturing crews following an annual scheduling capable for answering the hydraulic drilling of 20 wells per year [4].

Typical salinity average values (measured as total dissolved solids - TDS) for the shale gas flowback water from the Marcellus play are reported in the literature in a range of 120–157 k ppm [12,15,63]. However, it should be mentioned that other U.S. shale plays can present very distinct salt concentrations for the flowback water as shown in Table 1. For this reason, an initial mean value of 70 k ppm (or 70 g kg^{-1}) is considered for the feed salinity in the SEE/MEE system design. Nevertheless, it should be noted that the model is robust enough to guarantee optimal solutions for a large range of salinities and flowrates of the flowback water, underlining the facility for process scaling. Model performance and system sensitivity are evaluated under higher salinities in the next sections. Table 2 presents the problem data, while Fig. 1 shows the general superstructure proposed for the desalination of the high-salinity flowback water from shale gas fracking.

Additional problem data include the minimum pressure and temperature drop between evaporator effects equal to 0.1 kPa and 0.1 °C, respectively. Moreover, the minimum temperature approach between the outlet vapor and concentrated brine, as well as between the superheated vapor (*i.e.*, vapor after compression) and condensate (fresh water) in an evaporator effect is $\Delta T_{min} = 2$°C. The unknown minimum ideal temperature in the evaporation effect i is considered in a range of 1–100 °C to avoid operational problems (including rusting and fouling), while the saturated vapor pressure is restricted to 1–200 kPa. Most importantly, concentrate discharge salinity is specified to be equal to 300 g kg^{-1} (very close to salt saturation condition of ~350 g kg^{-1}) in order to achieve ZLD operation. In the case study, a factor of annualized capital cost (*fac*) of 0.16 is considered; this corresponds to 10% interest rate over a period of 10 years.

Table 2
Problem data for the case study based on the shale gas production.

Feed water (shale gas flowback water)	
Mass flowrate	37.5 $m^3\ h^{-1}$ (10.42 kg s^{-1})
Salinity	70 g kg^{-1}
Temperature	25 °C
Pressure	50 kPa
Multistage compressor with intercooling	
Type/material	Centrifugal/carbon steel
Isentropic efficiency	0.75
Heat capacity ratio	1.33
Maximum compression ratio	3 per stage
Cooling services temperature	20–25 °C
Specifications	
Brine salinity	300 g kg^{-1}
Cost data	
Electricity cost[a]	850.51 US$ $(kW\ year)^{-1}$
Cooling services cost	100 US$ $(kW\ year)^{-1}$
Factor of annualized capital cost	0.16 (10% - 10 years)

[a] Data obtained from Eurostat [71] database for industrial consumers in European Union (2015 - S1).

4.1. Optimizing the SEE/MEE system configuration

Several SEE/MEE system configurations are evaluated for their cost-effectiveness in obtaining concentrated brine at ZLD conditions and fresh water. In all cases, the minimization of the total annualized cost of the evaporation process is considered to be the objective function, which is composed by operational expenses and capital cost of investment. Initially, the system is optimized considering multiple-effect evaporation (MEE) without any additional equipment. In this case, steam at 120 °C and 50 kPa provided from an external source —C_{vapor} = 418.8 US$(year kW)$^{-1}$— is added to the first evaporation effect. The counter-current flow configuration is considered: the feed water (shale gas flowback water) is introduced in the last effect of the evaporator. In this way, the last evaporator effect is submitted to the lowest pressure and temperature of the system. The optimization of the MEE process is carried out by varying the number of evaporation effects. Thus, the optimal configuration obtained consists of 3 evaporator effects with heat transfer areas (and heat flow) equal to 204.16 m^2 (7086.95 kW), 176.91 m^2 (6896.88 kW) and 114.27 m^2 (6159.42 kW), respectively. The total annualized cost (TAC) is equal to 3237 k US$ year^{-1}, comprising 2579 k US$ year^{-1} related to operating expenses (OPEX) and 658 k US$ year^{-1} to capital cost of investment (CAPEX). Note that the evaporator with 2 effects presents a TAC equal to 4557 k US$ year^{-1} (*OPEX* = 4043k US$ year^{-1} and *CAPEX* = 514k US$ year^{-1}) while the evaporation equipment with 4 effects has a total cost of 4812 k US$ year^{-1} composed by *OPEX* = 2205k US$ year^{-1} and *CAPEX* = 2607k US$ year^{-1}. Therefore, the operating costs related to the consumed steam in the process is significantly reduced as the number of effects is increased (~36% of reduction from 2 to 3 effects) in the evaporator. This fact is related to the increment in the total heat transfer area that reduces the amount of heat required in the equipment. Note that, although the operational costs are decreasing with the increasing in the evaporator area, there is a threshold (3th effect) from that the increment in the capital costs needed do not compensate such reduction in the amount of energy.

4.2. Single-effect evaporation process with vapor recompression

The proposed model can be used to optimize a single-effect evaporation process with a single-stage compressor (SEE-SVR). In this situation, the evaporator heat transfer area (and heat flow) is equal to 782.99 m^2 (20,387.27 kW) and the compressor needed should has capacity of 1367.97 kW. Fig. 3 (*a*) shows the optimal solution obtained for the major decision variables for the SEE-SVR process. The total annualized cost for the SEE-SVR process is 2585 k US$ year^{-1}, including 1421 k US$ year^{-1} in capital cost and 1164 k US$ year^{-1} in electricity expenses. Thus, the TAC is 20.2% lower than the optimal solution obtained for the MEE process with external vapor source.

By the inclusion of a feed-condensate preheater to promote thermal integration, the heat transfer area of the single-effect evaporator (SEE-SVR including thermal integration) is increased for 834.17 m^2 (19,780.44 kW). The compressor capacity is also increased for 1452.19 kW to compensate for the heat flow required in the SEE-SVR including the thermal integration process. Moreover, the preheater required in the system has 4.80 m^2 of heat transfer area for exchanging 403.28 kW of heat between the feed and condensate streams. Fig. 4 shows the optimal solution obtained for the major decision variables for the SEE-SVR process including thermal integration. In this case, the capital cost of investment in equipment is equal to 1511 k US$ year^{-1}, and the operating expenses related to electricity are 1235 k US$ year^{-1}. Thus, the total annualized cost for the SEE-SVR configuration is equal to 2746 k US$ year^{-1}. Therefore, it is possible to achieve savings on total process costs around 15.2% in comparison with the optimal solution obtained for the MEE containing an external steam source (*i.e.*, 3-effect evaporator). However, the SEE-SVR system with thermal integration is 6.3% more expensive that the same process without preheated feed.

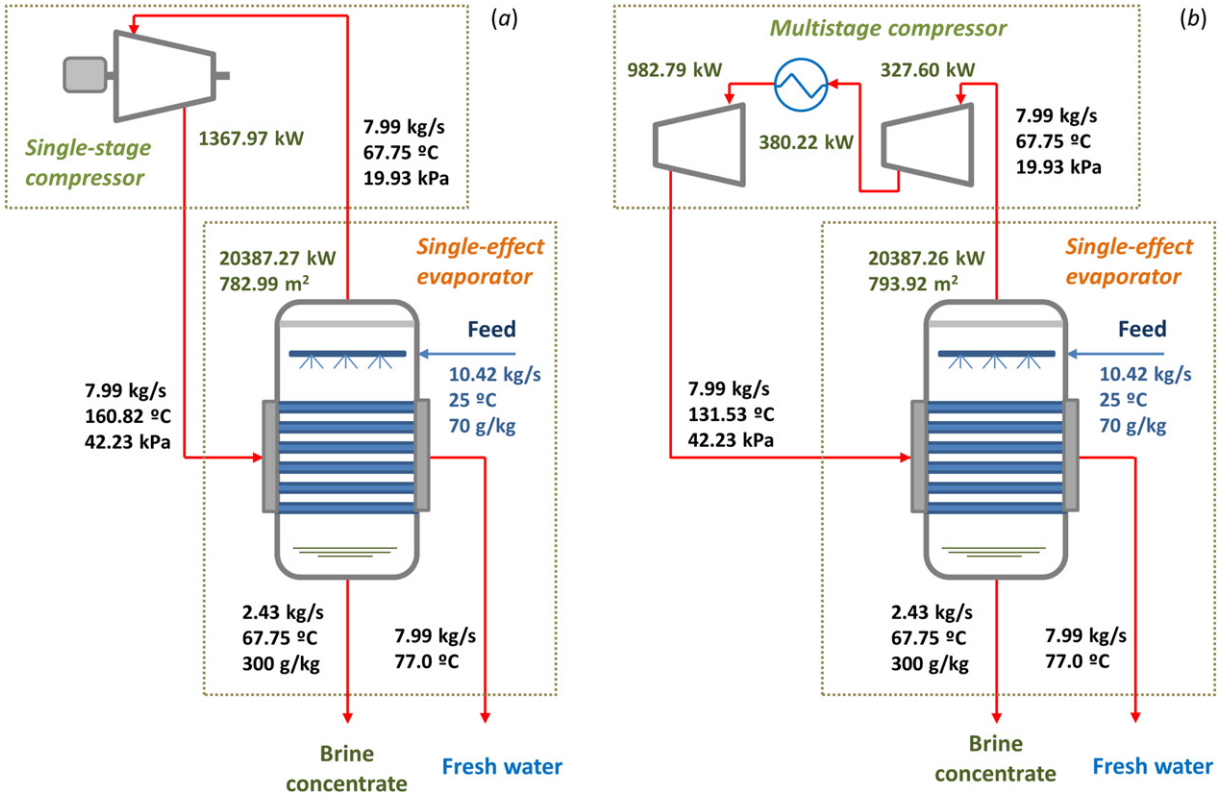

Fig. 3. Optimal solution obtained for the main decision variables for the single-effect evaporation process with (*a*) single-stage (SEE-SVR); and, (*b*) multistage (SEE-MVR) vapor recompression cycle.

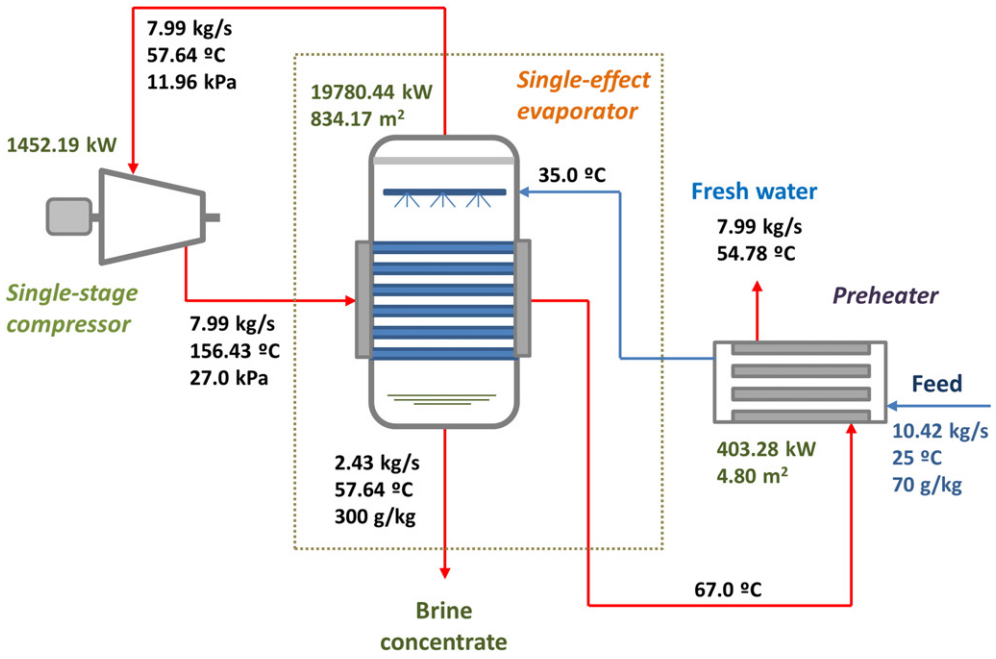

Fig. 4. Optimal solution obtained for the main decision variables for the single-effect evaporation process with single-stage vapor recompression cycle (SEE-SVR) and thermal integration.

This result is due to the increasing in both the capital costs and operational expenses obtained for the SEE-SVR configuration with a preheater.

Then, the model is used to optimize the single-effect evaporation process with a multistage compressor (SEE-MVR). In this case, the evaporator heat transfer area (and heat flow) is equal to 793.92 m^2 (20,387.26 kW). In addition, the process requires a 2-stage compressor with capacities of 327.60 kW and 982.79 kW, respectively. The multistage compressor demands 380.22 kW of energy related to cooling services. Fig. 3 (*b*) shows the optimal solution obtained for the major decision variables for the SEE-MVR process. The total annualized cost for the SEE-MVR process is 2576 k US$ $year^{-1}$, comprising 1423 k US$ $year^{-1}$ in capital cost and 1153 k US$ $year^{-1}$ in operational expenses. Thus, the TAC is 20.4% lower than the optimal solution obtained for the MEE process with external vapor source. Additionally, the SEE-MVR process is 6.2% more economical than SEE-SVR system and 0.4% cheaper than the SEE-SVR with thermal integration. In the last case, the decrease in the total annualized cost is due to the reduced operational expenses related to the use of a multistage compressor.

The SEE-MVR system including thermal integration presents a heat transfer area for evaporation (and heat flow) equal to 847.51 m^2 (19,780.44 kW). Furthermore, the optimal configuration requires a 2-stage compressor with capacities of 346.82 kW and 1040.45 kW, respectively. In this case, the multistage compressor consumes 395.16 kW of energy related to the intercooler. The feed-condensate preheater used in the process has 4.80 m^2 of heat transfer area for exchanging 403.28 kW of energy. The capital cost of investment in equipment is equal to 1515 k US$ $year^{-1}$, and the operating expenses related to the consumption of electricity are 1219 k US$ $year^{-1}$. Thus, the total annualized cost for the SEE-MVR configuration considering heat integration is equal to 2734 k US$ $year^{-1}$. Fig. 5 shows the optimal solution obtained for the major decision variables for the SEE-MVR process including thermal integration. It should be noted that the optimal SEE-MVR system configuration obtained is 6.2% more expensive than the same process without thermal integration. The increase in the total annualized cost is a consequence of the elevation in both capital costs and operational expenses. Note that the inclusion of a preheater in the SEE-MVR system reduces the vapor pressure and, consequently, the temperature in the evaporator. As a consequence, the heat flow provided by vapor recompression is reduced elevating the heat transfer area of evaporation. As expected, higher temperatures in the evaporator (as obtained for the SEE-MVR system without thermal integration) imply higher overall heat transfer coefficients and, consequently, lower heat transfer areas of evaporation.

On the other hand, the SEE-MVR system with thermal integration is 0.4% cheaper than the SEE-SVR system with preheated feed. The decrease in the total annualized cost is essentially due to the reduction in the work capacity and related operational expenses. In addition, it should be observed that the advantage of substituting the external vapor source —by a mechanical multistage compressor— is again verified in the SEE-MVR process with thermal integration. In this case, the optimal configuration obtained presents the total annualized cost 15.5% lower than the MEE system. Therefore, although the thermal integration does not provide better solutions for the single-stage evaporation with vapor recompression, the multistage compressor reduces operational costs —and consequently, the total annualized cost of the process— in all cases studied.

4.3. Multiple-effect evaporation process with vapor recompression

In this section, the multiple-effect evaporation system is designed considering the replacement of the external source of steam by a single-stage equipment for vapor recompression (MEE-SVR). In this case, the optimal solution is obtained for the MEE-SVR process composed of 2 effects of evaporation. The corresponding heat transfer areas (and heat flow) are equal to 343.84 m^2 (10,225.23 kW) and 282.21 m^2 (10,262.95 kW), respectively. Under this configuration, the process demands a single-stage compressor with the capacity of 820.41 kW. The operating expenses related to the consumption of electricity are equal to 698 k US$ $year^{-1}$, while the capital costs of investment in all process equipment are 1119 k US$ $year^{-1}$. Thus, the total annualized cost of the MEE system with this configuration is 1817 k US$ $year^{-1}$.

It should be observed that contrary to the MEE evaporation process with external steam source, the TAC is significantly increased as the number of effects is augmented in the multiple-effect evaporator. Consequently, if a 3-effect evaporator —with heat transfers areas (and heat flow) of 450.23 m^2 (6752.5 kW), 469.13 m^2 (6780.68 kW) and 304.19 m^2 (6697.59 kW), respectively— including mechanical vapor recompression (599.31 kW) is considered as the treatment plant, the total annualized cost will be increased to 2289 k US$ $year^{-1}$

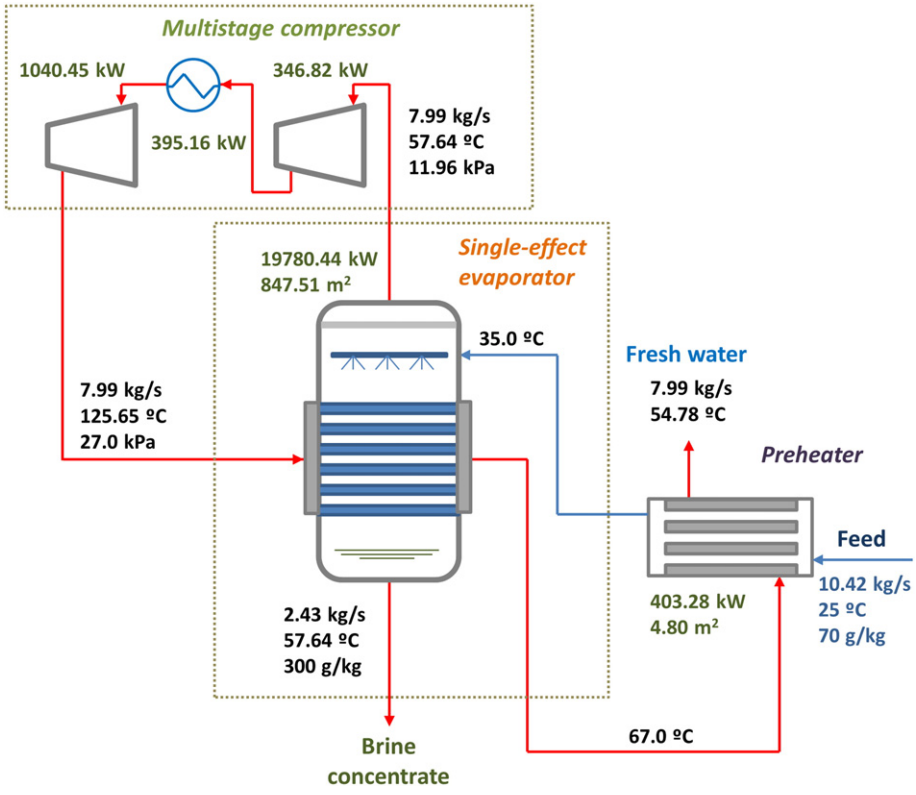

Fig. 5. Optimal solution obtained for the main decision variables for the single-effect evaporation process with multistage vapor recompression cycle (SEE-MVR) and thermal integration.

(*OPEX* = 510k US$ year^{-1} and *CAPEX* = 1779k US$ year^{-1}). This value corresponds to an increment of 25.9% in relation to the TAC obtained for the design with 2 effects of evaporation. Note that the increase in the total annualized cost is due to the need for bigger evaporator heat transfer areas, in which capital costs are significantly augmented when considering three (~59% more expensive) or more evaporation effects. On the other hand, the total annualized cost obtained considering the MEE-SVR system with 2 evaporation effects (and single-stage compressor) is 43.9% lower than the optimal solution found for the steam-driven MEE process. This reduction in the total costs is possible because, although a pressure manipulation equipment is used in the process —requiring an increased total heat transfer area of evaporation— the additional costs related to the inclusion in the MEE-SVR system of such mechanical compressor (including operational expenses and capital costs) do not exceed the expenses associated to external steam source (~270% more expensive than electricity expenses). Moreover, the MEE-SVR process is 29.4% cheaper than the best solution obtained for the single-effect evaporation process (*i.e.*, SEE-MVR without thermal integration). In this case, capital costs and operating expenses related to electricity consumption are both reduced when considering the multiple-effect evaporation process.

Afterwards, the MEE-SVR process is optimized considering thermal integration through the inclusion of flash tanks and feed-condensate preheater. In this case, the optimal configuration is again obtained with 2 effects in the evaporator. The heat transfer areas (and heat flow) of each evaporator effect are 246.25 m^2 (9718.77 kW) and 247.38 m^2 (9702.26 kW), respectively. Moreover, a single-stage mechanical compressor with the capacity of 823.11 kW is needed for meeting the energy required in the process. In this case, thermal integration is allowed in the process by using a preheater with area of 46.97 m^2 able to exchange 1774.31 kW of heat between the fresh water (distillate) and the feed water. Additionally, 2 flashing tanks —with volumes equal to 1.19 m^3 and 2.39 m^3, respectively— are used to separate the distillate vapor, providing a further energy recovery in the MEE-SVR system. Fig. 6 shows the optimal MEE-SVR process configuration obtained for this case study. The total annualized cost of the process with this configuration is 1689 k US$ year^{-1}, composed of 989 k US$ year^{-1} related to capital cost of investment in equipment and 700 k US$ year^{-1} to operating expenses of electricity consumption. Note that, the process designed with 3 evaporation effects has a total annualized cost of 1904 k US$ year^{-1}, composed of *OPEX* = 568k US$ year^{-1} and *CAPEX* = 1336k US$ year^{-1}. Therefore, analogously to the behavior observed for the MEE-SVR system without thermal integration, the process total annualized cost is significantly increased when more evaporator effects are considered in the system.

It should be highlighted that the MEE-SVR process design with thermal integration is 38.5% cheaper than the SEE-SVR system with preheating of the feed water. Moreover, the MEE-SVR process is 34.4% less expensive than the best solution obtained for the single-effect evaporation process (*i.e.*, SEE-MVR without thermal integration). In addition, this MEE-SVR configuration (*i.e.*, containing flash tanks and preheater) allows for reducing costs in 7.1%, comparing with the optimal solution obtained for the MEE-SVR without heat integration; and, 47.8% when compared with the optimal solution found for the MEE process. By analyzing these results, it is possible to observe that the heat recovery in the MEE-SVR process reduces significantly the total heat transfer area (~21% of reduction) required in the evaporator, in comparison with the MEE-SVR without thermal integration. The equipment size reduction is responsible for the considerable decrease in the capital cost of investment (~12% of reduction) and, subsequently, in the total annualized cost. Therefore, the thermal integration associated with the vapor recompression cycle in the MEE-SVR system is essential for enhancing energy efficiency and, consequently, for reducing process costs.

After the single-stage compression step, the developed mathematical model is used to optimize the multiple-effect evaporation system, considering multistage vapor recompression and thermal integration (MEE-MVR). Observe that the optimization is performed considering no pressure drop in the intercooler, and the inlet temperature in the

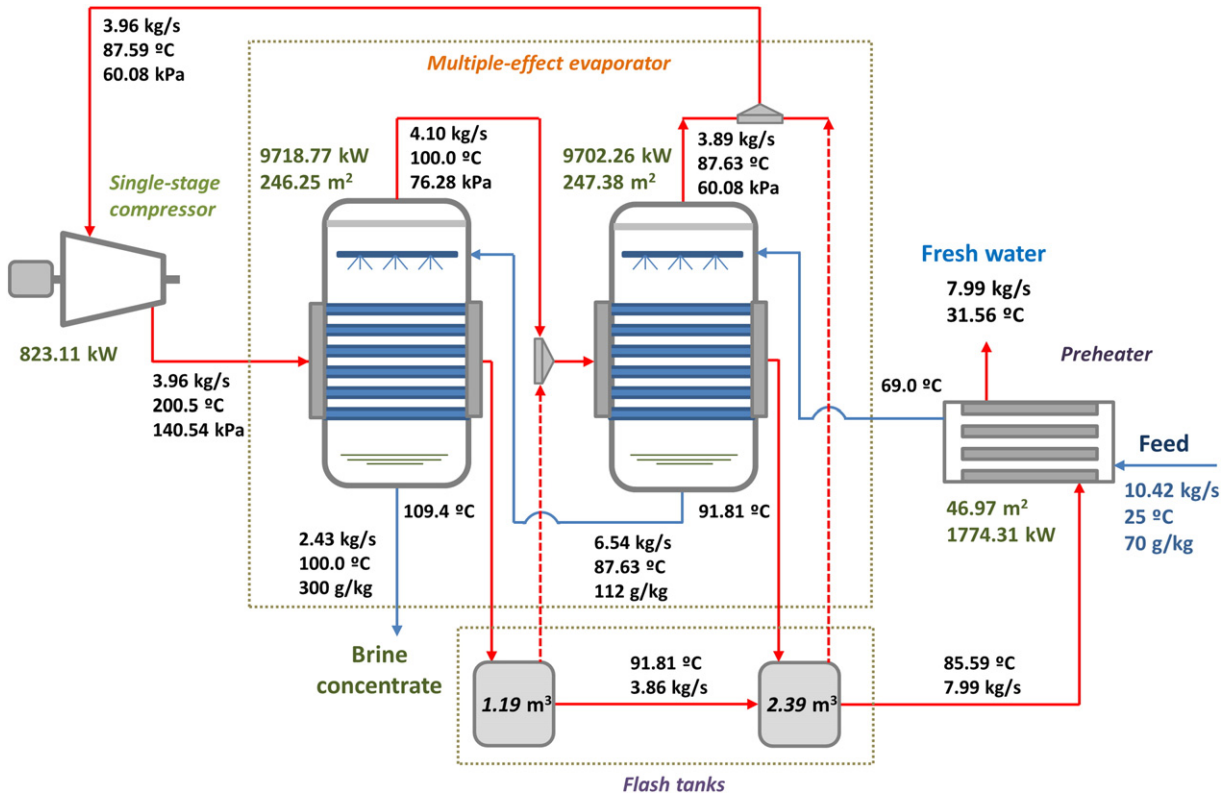

Fig. 6. Optimal solution obtained for the main decision variables for the multiple-effect evaporation process with single-stage vapor recompression cycle (MEE-SVR) and thermal integration.

first compression stage can be different from the inlet temperature in the subsequent stage. In this case, the optimal configuration obtained is composed of 2 effects of evaporation with heat transfer areas (and heat flows) equal to 346.77 m^2 (10,225.20 kW) and 282.21 m^2 (10,262.92 kW), respectively. In addition, the process requires a 2-stage compressor with capacities of 197.64 kW and 591.48 kW, respectively. The multistage compressor demands 176.59 kW of energy related to cooling services. The total annualized cost for the MEE-MVR system with this configuration is 1805 k US$ $year^{-1}$, comprising 1116 k US$ $year^{-1}$ of capital cost of investment and 689 k US$ $year^{-1}$ of operating expenses, related to cooling services and electricity consumed by the compressor.

It should be noted that the total annualized cost obtained for the MEE-MVR process represents 44.3% of savings in comparison with the MEE process (with an external source of vapor). Moreover, the MEE-MVR process is 29.9% cheaper than the best solution obtained for the single-effect evaporation process (*i.e.*, SEE-MVR without thermal integration). Additionally, the MEE-MVR system with thermal integration is 0.7% cheaper than the MEE-SVR system without feed preheating. The decrease in the total annualized cost is essentially due to the reduction in the work capacity and related electricity expenses.

Finally, the MEE-MVR process is optimized considering thermal integration by using intermediate flash tanks and feed-condensate preheater. In this case, the optimal configuration is again obtained with 2 effects in the evaporator system. The heat transfer areas (and heat flow) of each evaporation effect are 245.54 m^2 (9660.40 kW) and 268.67 m^2 (9646.39 kW), respectively. In addition, the optimal configuration requires a 2-stage compressor with capacities of 204.13 kW and 612.40 kW, respectively. In this case, the multistage compressor consumes 107.82 kW of energy related to the intercooler. A heat exchanger of 80.53 m^2 (1897.99 kW) is used to preheat the feed water, taking advantage of the energy from the condensate (fresh water). Additional energy is recovered in the MEE-MVR system by using 2 flashing tanks with capacities of 1.19 m^3 and 2.39 m^3, respectively. Fig. 7 shows the optimal MEE-MVR system configuration obtained for this case. The capital cost of investment in equipment is equal to 1015 k US$ $year^{-1}$, and the operating expenses related to the consumption of electricity are 705 k US$ $year^{-1}$. Thus, the total annualized cost for the MEE-MVR configuration considering heat integration is equal to 1720 k US$ $year^{-1}$.

Thus, the total annualized cost obtained for the MEE-MVR process with thermal integration represents 46.9% of savings in comparison with the MEE process (with an external source of vapor). The process presents a reduction of 46.9% in the cost of the produced fresh water, and 72.7% of decreasing in the energy consumed per cubic meter of produced water. Observe that the MEE-MVR process with this configuration is 33.2% cheaper than the best solution obtained for the single-effect evaporation process (*i.e.*, SEE-MVR without thermal integration). This reduction in the process expenses represent savings of ~33% in the cost of the cubic meter of fresh water; and, the decrease of ~39% in the electric power consumption per cubic meter of produced water. Moreover, the MEE-MVR process is 4.7% less expensive than the same process without thermal integration. Note that, in this case, the possibility of using the feed-distillate preheater allied to a larger compressor reduces significantly the heat transfer area of evaporation (~18% of reduction), compensating even the increment in the operational expenses related to the additional electricity consumption required by the process. Table 3 shows the optimal results obtained for the distinct evaporation systems configurations considered for the optimization of the desalination process.

Therefore, among all process configurations evaluated, the best option for the desalination of the shale gas flowback water (at 70 g kg^{-1}) is the MEE-SVR including thermal integration. In this case, the cost of the produced fresh water is 6.70 US$ per cubic meter, presenting an electric power consumption of 2.78 US$ per cubic meter of fresh water. However, it should be emphasized that the optimal configuration obtained is strongly dependent on the salinity of the flowback

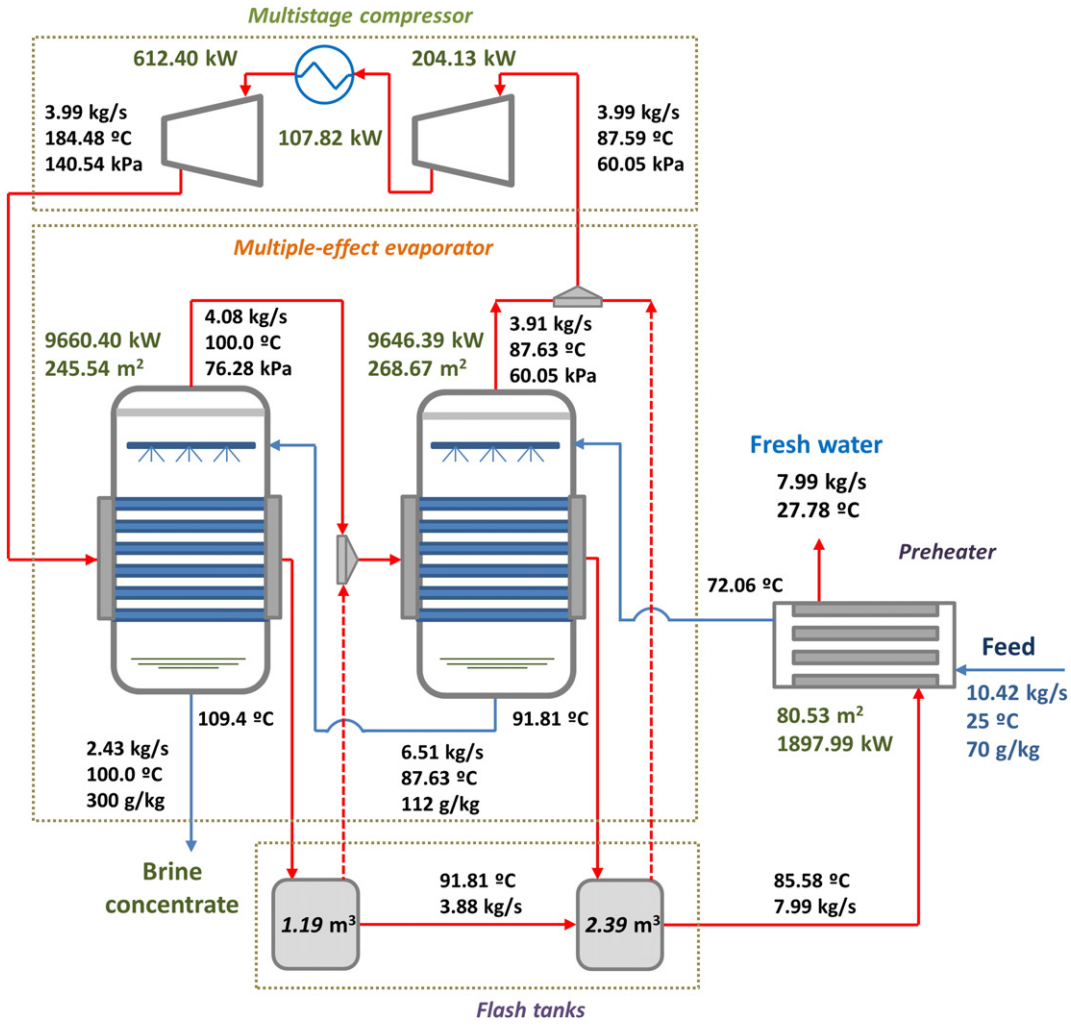

Fig. 7. Optimal solution obtained for the main decision variables for the multiple-effect evaporation process with multistage vapor recompression cycle (MEE-MVR) and thermal integration.

water to be treated. This dependence is studied in the following section. Lastly, it is remarked that in all SEE/MEE systems configurations studied, the specification of the brine salinity (300 g kg^{-1}) close to salt saturation condition allows for obtaining high recovery ratios of fresh water (0.77 in all cases) as it is shown in Table 3.

4.4. Analyzing the SEE/MEE model sensitivity

The proposed model can be used for the SEE/MEE process design considering a wide range of feed water salinities. A simple analysis of the SEE/MEE model sensitivity is performed to assess the influence of

Table 3
Optimal results obtained for the different evaporation systems configurations.[a]

Process configuration	Fresh water production cost (US$ m^{-3})	Steam/electric power consumed (US$ m^{-3})	Total annualized cost (kUS$ $year^{-1}$)
Multiple-effect evaporation with external steam source (MEE)	12.85	10.24	3237.1
Single-effect evaporation with single-stage vapor recompression (SEE-SVR)	10.26	4.62	2584.6
SEE-SVR including thermal integration	10.90	4.90	2746.0
Single-effect evaporation with multistage vapor recompression (SEE-MVR)	10.22	4.57	2575.7
SEE-MVR including thermal integration	10.85	4.84	2734.1
Multiple-effect evaporation with single-stage vapor recompression (MEE-SVR)	7.21	2.77	1817.3
MEE-SVR including thermal integration	6.70	2.78	1688.6
Multiple-effect evaporation with multistage vapor recompression (MEE-MVR)	7.16	2.73	1804.6
MEE-MVR including thermal integration	6.83	2.80	1720.3

[a] Results obtained by specifying brine salinity levels near to salt saturation concentration (i.e., 300 g kg^{-1}). In all cases, this consideration allows to recover concentrated brine at 2.43 kg s^{-1} and fresh water production ratio at 7.99 kg s^{-1} (Conversion ratio: $CR = F_{condensate}/F_{feed} = 0.77$).

the feed water salinity on system performance and total process costs. Thus, the optimal solutions found in the design step (considering feed water salinity equal to 70 g kg^{-1}) for the single and multiple-effect systems configurations have been evaluated under salinity conditions varying from 10 to 220 g kg^{-1} (10–220 k ppm). In all cases, the brine specification remains the same (*i.e.*, 300 g kg^{-1}) to achieve discharges close to ZLD conditions. It should be remembered that the consideration of higher salinities implies the need for lower brine concentration, since the system is always designed to achieve the same outlet condition (*i.e.*, brine concentrate near to salt saturation condition). The results obtained for the SEE-MVR system without thermal integration present a linear decrease in the total annualized cost of the process, as higher salinities are considered for the feed water. Fig. 8 (*a*) displays the effect of the flowback water salinity on the SEE-MVR process costs. The total annualized cost of the system is equal to 3167 k US$ $year^{-1}$ for feed salinity of 10 g kg^{-1}. Under more elevated concentrations, a significant reduction in the total costs is observed for this configuration. At feed salinity of 220 g kg^{-1}, the total annualized cost of the process is 1147 k US$ $year^{-1}$. This value represents a diminution of approximately 64% in comparison with the optimal solution found for the process at lower salinity condition. In this case, the system configuration exhibits a proportional lessening in both curves for capital costs and operational expenses. This fact is due to the smaller equipment size (~61% of reduction between the evaluated extremes points) and the consequent need for lower energy consumption (~67% of savings in operational expenses). Therefore, the performance of the system (measured by the total evaporation area and compression capacity) is considerably affected for the shale gas flowback water salinity. In this case, the evaporator area is reduced by ~69%, whereas the compression work is decreased by ~66%.

The total costs for the MEE-MVR system with thermal integration for different feed water salinities are shown in Fig. 8 (*b*). In this case, the reduction observed in the total annualized cost for the salinity extreme conditions (10 and 220 g kg^{-1}) is not so expressive as in the single-effect process. For the first salinity, the MEE-MVR system presents a total annualized cost of 1959 k US$ $year^{-1}$, which is composed by 1166 k US$ $year^{-1}$ related to capital costs and 793 k US$ $year^{-1}$ associated to operational expenses. For the feed water with 220 g kg^{-1}, the total annualized cost of the system is equal to 1216 k US$ $year^{-1}$ (*OPEX* = 391k US$ $year^{-1}$ and *CAPEX* = 825k US$ $year^{-1}$). This value constitutes a decrease of ~38% in the total annualized cost, (~29% in the capital cost and ~51% in the operational expenses) when both conditions are compared. Concerning the system performance, the compression work is substantially more affected by the increase in the feed water salinity over the total evaporation area. Therefore, the compression work is decreased by ~52% while the evaporator area is reduced by ~29%.

The MEE-SVR process with thermal integration is the last system to be analyzed. The results obtained for this configuration are displayed in Fig. 8 (*c*). In this case, the total annualized cost is equal to 1925 k US$ $year^{-1}$ for the treatment of the feed water at 10 g kg^{-1}. The total annualized cost comprises 1147 k US$ $year^{-1}$ associated to capital costs and 778 k US$ $year^{-1}$ to operational expenses. At feed water salinity of 220 g kg^{-1}, the total annualized cost of the MEE-SVR process is 1839 k US$ $year^{-1}$ (*OPEX* = 238k US$ $year^{-1}$ and

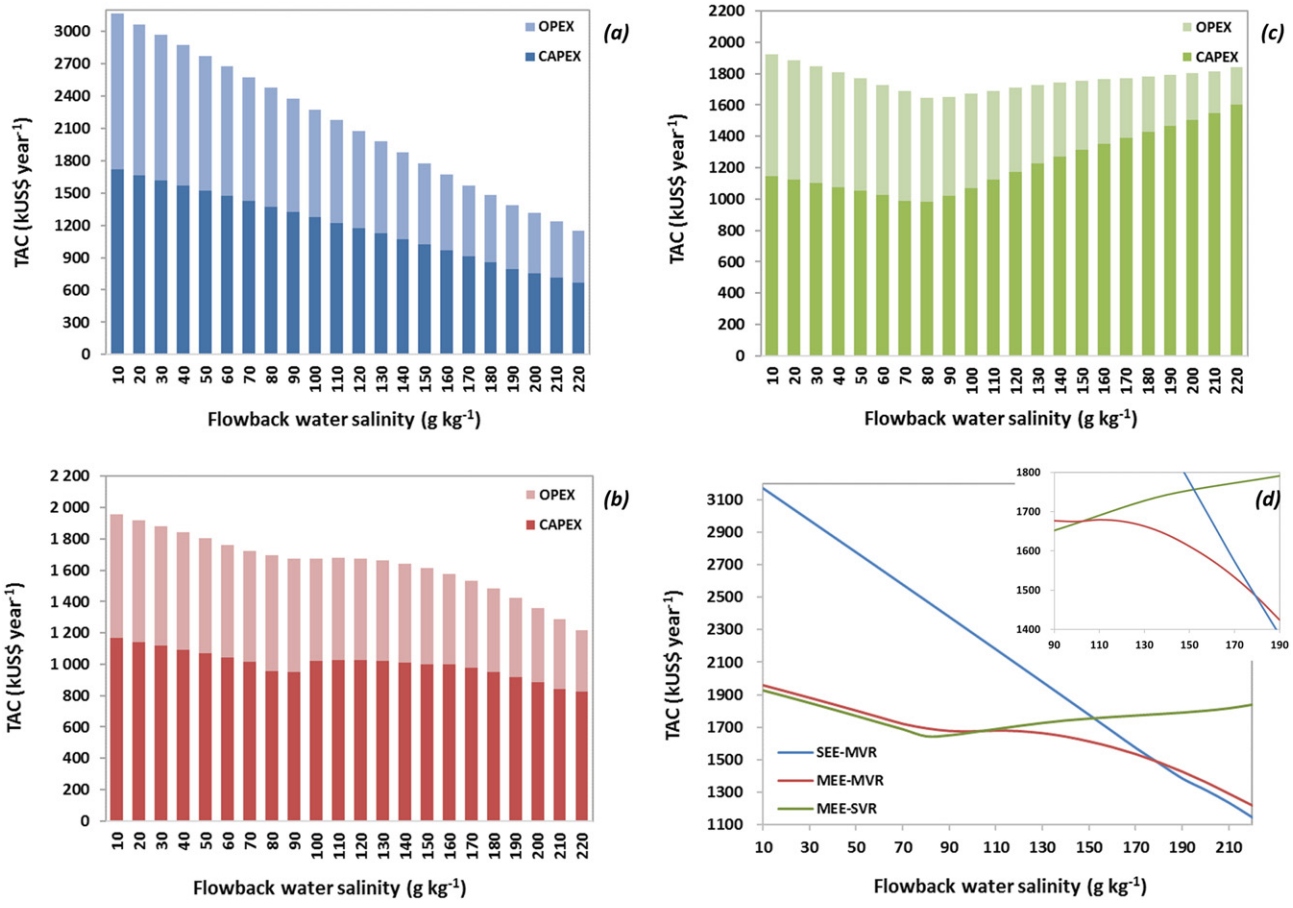

Fig. 8. Effect of the flowback water salinity on the process costs of: (*a*) single-effect evaporation system with multistage vapor recompression cycle (SEE-MVR); (*b*) multiple-effect evaporation system with multistage vapor recompression cycle (MEE-MVR) and thermal integration; (*c*) multiple-effect evaporation system with single-stage vapor recompression cycle (MEE-SVR) and thermal integration; and, (*d*) comparison between the total annualized costs obtained for the processes SEE-MVR, MEE-MVR and MEE-SVR under different feed salinity conditions.

CAPEX = 1601k US$ year^{-1}). This value represents a reduction of ~5% in comparison with the optimal solution found for the process at 10 g kg^{-1}. The system with this configuration presents ~69% of savings in operational expenses. On the other hand, the capital cost of investment is increased by ~40%. This fact is due to the significant increase in the total evaporation area (~93%), whereas the compression work is reduced by ~70%. However, the MEE-SVR system configuration exhibits an inflection point at the feed water salinity equal to 80 g kg^{-1}. Therefore, the process presents a minimum total annualized cost of 1646 k US$ year^{-1} under this condition.

Finally, Fig. 8 (*d*) shows the comparison between the total annualized costs obtained for the processes SEE-MVR, MEE-MVR and MEE-SVR under different feed salinity conditions. In this figure, it is possible to observe that the MEE-SVR process (with thermal integration) presents the lower total costs at salinities between 10 and 100 g kg^{-1}. In this concentration range, the SEE-MVR (without thermal integration) is the most expensive process for the treatment of the shale gas flowback water. Between the salinities of 100 to 150 g kg^{-1}, the MEE-MVR system (with thermal integration) becomes the most economical process to achieve brine discharges close to ZLD conditions. From salinities higher than 150 g kg^{-1}, the MEE-SVR system is the less beneficial process. Note that the MEE-SVR system presents the lower compared total annualized cost for the feed salinity at 70 g kg^{-1}. Interestingly, the SEE-MVR system has the lower total annualized cost for salinities higher than 180 g kg^{-1}. Observe that the SEE-MVR process is widely used in the seawater desalination industry, in which there is no need to achieve ZLD conditions.

4.5. Simulating the MEE process

To verify the accuracy of the proposed mathematical programming model, a simulation of the process has been carried out using the commercial software Aspen HYSYS (version V8.8). With this aim, the MEE-MVR superstructure shown in Fig. 1 has been simulated considering steady state conditions. The resulting MEE-MVR process flow diagram in Aspen HYSYS is displayed in Fig. 9. The MEE-MVR system has been selected due to its elevated complexity in comparison with the other systems designed.

The thermodynamic package NTRL-electrolytes has been chosen for the process simulation. Moreover, the results obtained for the decision variables (*i.e.*, inlet and outlet pressures and temperatures, and mass flowrates) in the design step (shown in Fig. 7) have been introduced in the simulator to estimate the work capacities or heat flows of all equipment. A reasonably good agreement has been observed between the design and simulated values for the MEE-MVR process. The simulation results showed that the compressor stages should have the capacities of 208.7 kW and 618.3 kW, respectively. In this case, the intercooler consumes 111.8 kW of energy. These values present differences of 0.9%, 2.2% and 3.7%, respectively, in relation to the design ones. In the simulation, the effects of the evaporator present heat flows equal to 9555 kW and 9652 kW, respectively. The difference between the values obtained from the model and the simulated ones are equal to 1.2% and 0.1%, respectively.

The simulation of the preheater has also shown high precision with the modeled results. The difference between the two values is equal to

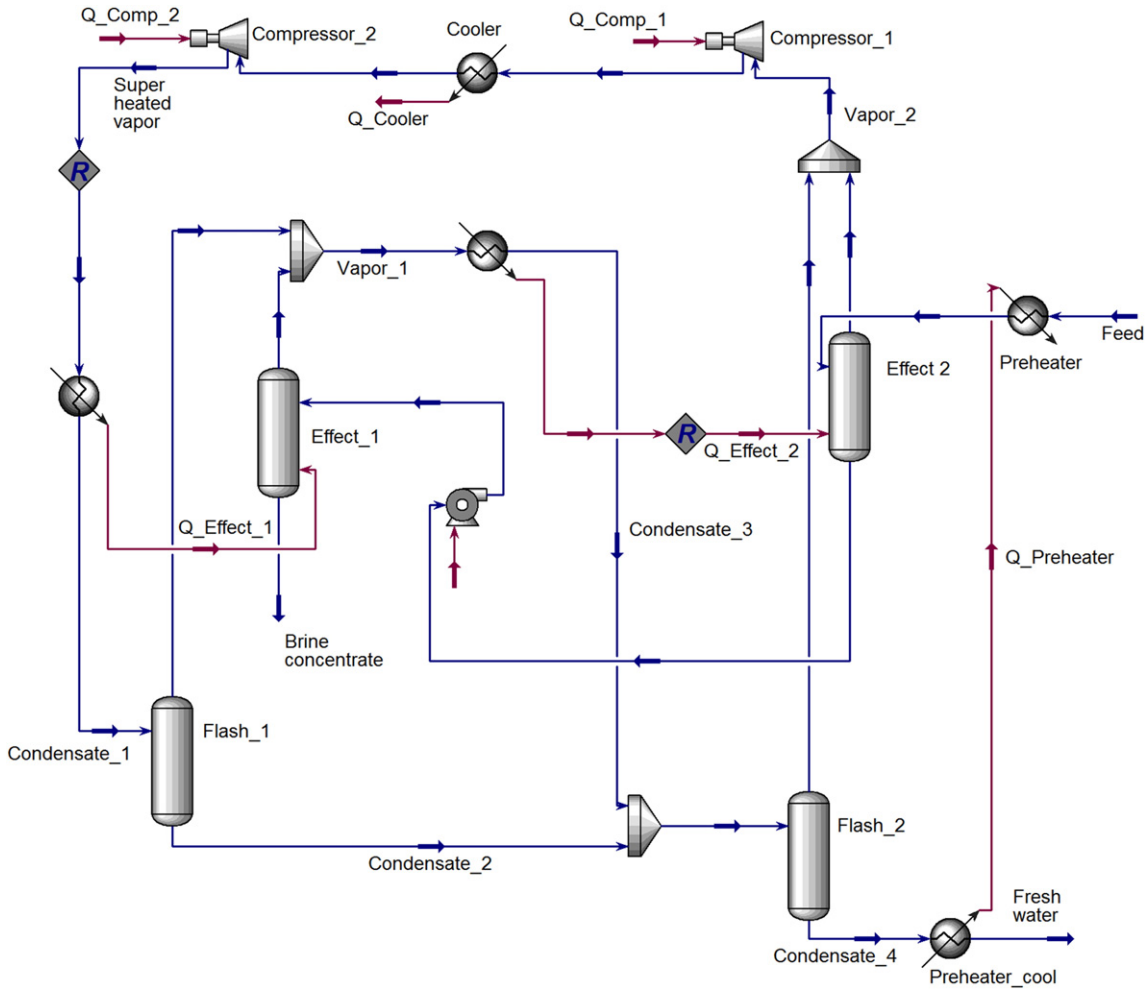

Fig. 9. MEE-MVR process flow diagram in Aspen HYSYS used to validate the results obtained in the system design step.

0.8%. In this case, the heat duty simulated is equal to 1882 kW. Moreover, all the remaining simulated values (including some inlet or outlet temperatures, pressures and mass flowrates) exhibit variations in relation to the design values lower than 1%. It should be highlighted that the low differences obtained between the modeling and simulation are mainly due to the use of correlations to estimate some decision variables in the mathematical model.

4.6. Computational aspects

The proposed NLP model for the optimal design of SEE/MEE systems was implemented in GAMS software (version 24.6.1) and optimized using CONOPT solver [67]. It is emphasized that the optimization of NLP problems using reduced gradient method-based solver —like CONOPT— cannot guarantee global optimal solutions, unless the problem is convex (*i.e.*, convex objective function and constraints) [68]. However, good solutions can be expected due to the problem size and robustness of the proposed model. All examples studied were solved using a computer with an Intel Core i5-2520 M 2.5 GHz processor and 8 GB RAM running Windows 8.1. The CPU time did not exceed 1 s for any of the CONOPT optimizations. The statistics of the SEE/MEE model and computational efforts for solving the problem are reported in Table 4.

It should be highlighted that the imposition of limits (*i.e.*, lower and upper bounds) on all decision variables are essential to solve the SEE/MEE model. These bounds should be carefully defined to guarantee that all functions can be properly evaluated by the NLP solver. Thus, it is crucial to ensure all achievable flexibility in the lower and upper bounds. Additionally, it is very important to provide good starting points by setting level values on all decision variables. In general, a NLP solver (CONOPT) is not able to find optimal or at least feasible solutions when bad starting points are chosen.

5. Conclusions

A new optimization model for the simultaneous synthesis of SEE/MEE systems is proposed, including mechanical vapor recompression and thermal integration. To the best of our knowledge, this is the first work proposing the SEE/MEE process (including MVR and thermal integration) for the treatment of high-salinity flowback water from shale gas production. The mathematical model is formulated as a NLP problem and solved using GAMS software, by minimizing the total annualized cost of desalinating the shale gas flowback water. For this purpose, a multiple-effect superstructure is developed including several effects of evaporation and multistage mechanical compression. In addition, condensate flashing tanks and feed/condensate preheater are used to enhance energy recovery. As the compressor with intercooling is an electricity-driven device, no additional energy source is needed in the SEE/MEE process. Nevertheless, the mathematical model allows for easily changing the energy supply if electricity services are not available.

The optimal SEE/MEE configuration should achieve high recovery ratio of produced fresh water and brine near to ZLD condition —through the specification of the outflow brine salinity near to salt saturation conditions—, by minimizing the process costs. The objective function accounts for the capital cost of investment in equipment, and operating expenses related to cooling services and electricity consumption. It is worth noting that improving the process cost-effectiveness by reducing brine discharges allows decreasing the environmental impacts associated to energy consumption and waste disposal.

It is remarked that the SEE/MEE design considering MVR and thermal integration is a complex process, seeking to find the optimal system configuration with minimum heat transfer area and use of energy services. All streams properties are unknown decision variables for the process design. In addition to the raised number of variables and constraints, the high non-convexity and nonlinearity of the cost correlations further increase the model complexity.

First, the SEE and MEE systems have been compared in terms of their applicability to produce fresh water and achieve ZLD conditions. Among all process configurations studied, the MEE-SVR including thermal integration has presented the lower total annualized cost of process (1689 k US$ year^{-1}). Therefore, this configuration represents the best option for the desalination of the shale gas flowback water with salinity of 70 g kg^{-1}. The MEE-SVR process including thermal integration also presents the lower value for the cost of the produced fresh water (6.70 US$ per cubic meter). However, all configurations evaluated have obtained high recovery ratios of fresh water (77% in all cases), and they have successfully achieved brine outlet specification (*i.e.*, brine discharges near ZLD conditions).

Sensitivity analysis has been performed to assess the optimal SEE/MEE process configuration and performance under distinct feed water salinity conditions. The results obtained highlight the robustness of the proposed model to cost-effectively optimize SEE/MEE systems under low and high feed water concentrations. Moreover, sensitivity analysis emphasizes that the optimal process configuration is strongly dependent of the salinity of the flowback water to be treated. The MEE-MVR system configuration is the most beneficial process for the treatment of feed water at lower salinities (10–100 g kg^{-1}), whereas the SEE-MVR is the most economical at salinities higher than 180 g kg^{-1}.

Lastly, simulation results by using Aspen HYSYS emphasize the accuracy of the proposed model for synthesizing the MEE-MVR system. A good agreement has been observed between the design and simulated values, showing high model accuracy in relation to realistic data of design. The difference between the design and simulated performance parameters (including heat flows and compression work) of the process have not exceeded 4%. This small difference is attributed to the correlations (of the data obtained from HYSYS-OLI by using a more rigorous

Table 4
Model statistics and computational efforts for solving the problem considering different process configurations.[a]

SEE/MEE model	Continuous variables	Constraints (equality and inequality)	Jacobian elements (non-zeros)/non-linear
Multiple-effect evaporation with external steam source (MEE)	31	88	226/83
Single-effect evaporation with single-stage vapor recompression (SEE-SVR)	42	47	123/46
SEE-SVR including thermal integration	53	57	158/60
Single-effect evaporation with multistage vapor recompression (SEE-MVR)	51	60	160/61
SEE-MVR including thermal integration	62	70	195/75
Multiple-effect evaporation with single-stage vapor recompression (MEE-SVR)	60	72	189/67
MEE-SVR including thermal integration	88	100	285/109
Multiple-effect evaporation with multistage vapor recompression (MEE-MVR)	70	85	226/82
MEE-MVR including thermal integration	97	113	322/124

[a] The CPU time for all cases studied is lower than 1 s, optimizing by using the CONOPT solver under GAMS software.

thermodynamic package for electrolytes) used in the mathematical model formulation.

Further development of the process technology is needed to ensure the best possibilities for the treatment of the shale gas flowback water. Thus, future works include the study of the influence of the overall heat transfer coefficient on the process configuration and performance; analysis of the uncertainty associated to the concentration data of the wells; and, consideration of the salinity variation as a function of the exploration time. Finally, the assessment of environmental impacts following LCA principles should also be considered for the optimal design of more environmentally conscious processes.

Nomenclature

Roman letters

A	heat transfer area, m^2
BPE	boiling point elevation, °C
$CAPEX$	capital expenses, kUS$ $year^{-1}$
Cc	cost parameter for the cooling services, US$ $(kW\ year)^{-1}$
Cp	specific heat, kJ $(kg\ °C)^{-1}$
CPO	cost of equipment unit, kUS$
CR_{max}	maximum compression ratio
Ec	cost parameter for electricity, US$ $(kW\ year)^{-1}$
fac	factor of annualized capital cost
F	mass flowrate, kg s^{-1}
FBM	correction factor for the capital cost
FP	parameter for the capital cost estimation
H	specific enthalpy, kJ kg^{-1}
$LMTD$	logarithmic mean temperature difference
$OPEX$	operational expenses, kUS$ $year^{-1}$
P	pressure, kPa
ΔP_{min}	minimum pressure approach, kPa
Q	heat flow, kW
r	fractional interest rate per year
S	salinity, g kg^{-1}
T	temperature, °C
t	retention time in the flash tanks, min
ΔT_{min}	minimum temperature approach, °C
TAC	total annualized cost, kUS$ $year^{-1}$
U	overall heat transfer coefficient, kW m^{-2} K^{-1}
V	volume, m^3
XS	Salt mass fraction
y	number of years
W	compression work, kW

Subscripts

c	condensate
i	evaporator effects
j	compressor stages

Superscript

c	compressor
is	isentropic
m	mixture
cv	condensate vapor
sv	saturated vapor
spv	superheated vapor

Acronyms

CEPCI	Chemical Engineering Plant Cost Index
GAMS	General Algebraic Modeling System
LCA	Life Cycle Assessment
MEE	Multiple-Effect Evaporation
MSF	Multistage Flash
MVR	Mechanical Vapor Recompression
NLP	Nonlinear Programming
RO	Reverse Osmosis
SEE	Single-Effect Evaporation
TDS	Total Dissolved Solids
TVR	Thermal Vapor Recompression
ZLD	Zero Liquid Discharge

Greek letters

γ	heat capacity ratio
η	isentropic efficiency
θ	temperatures difference, °C
λ	latent heat of vaporization, kJ kg^{-1}
ρ	water density, kg m^{-3}

Acknowledgements

This project has received funding from the European Union's Horizon 2020 Research and Innovation Programme under grant agreement No. 640979. The financial support provided by the National Council for Scientific and Technological Development of Brazil (CNPq), under process No. 233953/2014-0 is also gratefully acknowledged.

References

[1] J. Gao, F. You, Shale gas supply chain design and operations toward better economic and life cycle environmental performance: MINLP model and global optimization algorithm, ACS Sustain. Chem. Eng. 3 (2015) 1282–1291, http://dx.doi.org/10.1021/acssuschemeng.5b00122.
[2] B. Xiong, A.L. Zydney, M. Kumar, Fouling of microfiltration membranes by flowback and produced waters from the Marcellus shale gas play, Water Res. (2016), http://dx.doi.org/10.1016/j.watres.2016.04.049.
[3] T. Stephenson, J.E. Valle, X. Riera-Palou, Modeling the relative GHG emissions of conventional and shale gas production, Environ. Sci. Technol. 45 (2011) 10757–10764, http://dx.doi.org/10.1021/es2024115.
[4] L.F. Lira-Barragán, J.M. Ponce-Ortega, G. Guillén-Gosálbez, M.M. El-Halwagi, Optimal water management under uncertainty for shale gas production, Ind. Eng. Chem. Res. 55 (2016) 1322–1335, http://dx.doi.org/10.1021/acs.iecr.5b02748.
[5] J.-P. Nicot, B.R. Scanlon, Water use for shale-gas production in Texas, U.S. Environ. Sci. Technol. 46 (2012) 3580–3586, http://dx.doi.org/10.1021/es204602t.
[6] C.L. Weber, C. Clavin, Life cycle carbon footprint of shale gas: review of evidence and implications, Environ. Sci. Technol. 46 (2012) 5688–5695, http://dx.doi.org/10.1021/es300375n.
[7] M.S. Mauter, P.J.J. Alvarez, A. Burton, D.C. Cafaro, W. Chen, K.B. Gregory, G. Jiang, Q. Li, J. Pittock, D. Reible, J.L. Schnoor, Regional variation in water-related impacts of

shale gas development and implications for emerging international plays, Environ. Sci. Technol. 48 (2014) 8298–8306, http://dx.doi.org/10.1021/es405432k.
[8] A. Vengosh, N. Warner, R. Jackson, T. Darrah, The effects of shale gas exploration and hydraulic fracturing on the quality of water resources in the United States, Procedia Earth Planet. Sci. 7 (2013) 863–866, http://dx.doi.org/10.1016/j.proeps.2013.03.213.
[9] E. Barbot, N.S. Vidic, K.B. Gregory, R.D. Vidic, Spatial and temporal correlation of water quality parameters of produced waters from devonian-age shale following hydraulic fracturing, Environ. Sci. Technol. 47 (2013) 2562–2569, http://dx.doi.org/10.1021/es304638h.
[10] C. He, X. Wang, W. Liu, E. Barbot, R.D. Vidic, Microfiltration in recycling of Marcellus shale flowback water : solids removal and potential fouling of polymeric microfiltration membranes, J. Membr. Sci. 462 (2014) 88–95, http://dx.doi.org/10.1016/j.memsci.2014.03.035.
[11] M.A. Cluff, A. Hartsock, J.D. MacRae, K. Carter, P.J. Mouser, Temporal changes in microbial ecology and geochemistry in produced water from hydraulically fractured Marcellus shale gas wells, Environ. Sci. Technol. 48 (2014) 6508–6517, http://dx.doi.org/10.1021/es501173p.
[12] H.R. Acharya, C. Henderson, H. Wang, Cost effective recovery of low-TDS frac flowback water for re-use, Glob. Res. 1–100 (2011).
[13] C.E. Clark, R.M. Horner, C.B. Harto, Life cycle water consumption for shale gas and conventional natural gas supporting information, Environ. Sci. Technol. 47 (2013) 1–9, http://dx.doi.org/10.1021/es4013855.
[14] J.B. Jacquet, Review of risks to communities from shale energy development, Environ. Sci. Technol. 48 (2014) 8321–8333, http://dx.doi.org/10.1021/es404647x.
[15] L.O. Haluszczak, A.W. Rose, L.R. Kump, Geochemical evaluation of flowback brine from Marcellus gas wells in Pennsylvania, USA, Appl. Geochem. 28 (2013) 55–61, http://dx.doi.org/10.1016/j.apgeochem.2012.10.002.
[16] I.E. Cafaro, D.C. Grossmann, Strategic planning, design, and development of the shale gas supply chain network, AICHE J. 60 (2014) 6–21, http://dx.doi.org/10.1002/aic.14405.
[17] B.G. Rahm, S.J. Riha, Toward strategic management of shale gas development: regional, collective impacts on water resources, Environ. Sci. Pol. 17 (2012) 12–23, http://dx.doi.org/10.1016/j.envsci.2011.12.004.
[18] L. Yang, I.E. Grossmann, J. Manno, Optimization models for shale gas water management, AIChE J. 60 (2014) 3490–3501, http://dx.doi.org/10.1002/aic.14526.
[19] X. Zhang, A.Y. Sun, I.J. Duncan, Shale gas wastewater management under uncertainty, J. Environ. Manag. 165 (2016) 188–198, http://dx.doi.org/10.1016/j.jenvman.2015.09.038.
[20] P.L. Staddon, M.H. Depledge, Fracking cannot be reconciled with climate change mitigation policies, Environ. Sci. Technol. (2015) 8269–8270, http://dx.doi.org/10.1021/acs.est.5b02441.
[21] D.L. Shaffer, L.H. Arias Chavez, M. Ben-Sasson, S. Romero-Vargas Castrillón, N.Y. Yip, M. Elimelech, Desalination and reuse of high-salinity shale gas produced water: drivers, technologies, and future directions, Environ. Sci. Technol. 47 (2013) 9569–9583, http://dx.doi.org/10.1021/es401966e.
[22] L.M. Camacho, L. Dumée, J. Zhang, J. Li, M. Duke, J. Gomez, S. Gray, Advances in membrane distillation for water desalination and purification applications, Water 5 (2013) 94–196, http://dx.doi.org/10.3390/w5010094.
[23] I.S. Al-Mutaz, Features of multi-effect evaporation desalination plants, Desalin. Water Treat. 54 (2015) 3227–3235, http://dx.doi.org/10.1080/19443994.2014.910842.
[24] İ. Halil, M.S. Söylemez, Design and computer simulation on multi-effect evaporation seawater desalination system using hybrid renewable energy sources in Turkey, Desalination 291 (2012) 23–40, http://dx.doi.org/10.1016/j.desal.2012.01.022.
[25] G. Gautami, S. Khanam, Selection of optimum configuration for multiple effect evaporator system, Desalination 288 (2012) 16–23, http://dx.doi.org/10.1016/j.desal.2011.12.005.
[26] P. Druetta, P. Aguirre, S. Mussati, Optimization of multi-effect evaporation desalination plants, Desalination 311 (2013) 1–15, http://dx.doi.org/10.1016/j.desal.2012.10.033.
[27] P. Druetta, P. Aguirre, S. Mussati, Minimizing the total cost of multi effect evaporation systems for seawater desalination, Desalination 344 (2014) 431–445, http://dx.doi.org/10.1016/j.desal.2014.04.007.
[28] I.S. Al-Mutaz, I. Wazeer, Comparative performance evaluation of conventional multi-effect evaporation desalination processes, Appl. Therm. Eng. 73 (2014) 1194–1203, http://dx.doi.org/10.1016/j.applthermaleng.2014.09.025.
[29] O.A. Hamed, K. Ba-mardouf, H. Al-Washmi, K. Al-Shail, H. Abdalla, A. A. Al-, Modeling and simulation of multistage flash distillation process — Part II, Technical Report (2004) 1–49.
[30] O.A. Hamed, M.A.K. Al-Sofi, G.M. Mustafa, K. Ba-Mardouf, H. Al-Washmi, Modeling and simulation of multistage flash distillation process, Technical Report (1999) 1–44.
[31] A.S. Nafey, H.E.S. Fath, A.A. Mabrouk, Thermoeconomic analysis of multi stage flash-thermal vapor compression (MSF-TVC) desalination process, Tenth International Water Technology Conference (2006) 189–203.
[32] F.M.H. El-Dessouky, H. Ettouney, H. Al-Fulaij, Multistage flash desalination combined with thermal vapor compression, Chem. Eng. Process. Process Intensif. 39 (2000) 343–356.
[33] C. Fritzmann, J. Löwenberg, T. Wintgens, T. Melin, State-of-the-art of reverse osmosis desalination, Desalination 216 (2007) 1–76, http://dx.doi.org/10.1016/j.desal.2006.12.009.
[34] L.F. Greenlee, D.F. Lawler, B.D. Freeman, B. Marrot, P. Moulin, P. Ce, Reverse osmosis desalination: water sources, technology, and today's challenges, Water Res. 43 (2009) 2317–2348, http://dx.doi.org/10.1016/j.watres.2009.03.010.
[35] S. Zhao, L. Zou, C.Y. Tang, D. Mulcahy, Recent developments in forward osmosis: opportunities and challenges, J. Membr. Sci. 396 (2012) 1–21, http://dx.doi.org/10.1016/j.memsci.2011.12.023.
[36] Y. Lu, Y. Hu, X. Zhang, L. Wu, Q. Liu, Optimum design of reverse osmosis system under different feed concentration and product specification, J. Membr. Sci. 287 (2007) 219–229, http://dx.doi.org/10.1016/j.memsci.2006.10.037.
[37] N.M. Al-Bastaki, A. Abbas, Modeling an industrial reverse osmosis unit, Desalination 126 (1999) 33–39, http://dx.doi.org/10.1016/S0011-9164(99)00152-6.
[38] G. Chen, Z. Wang, L.D. Nghiem, X.M. Li, M. Xie, B. Zhao, M. Zhang, J. Song, T. He, Treatment of shale gas drilling flowback fluids (SGDFs) by forward osmosis: membrane fouling and mitigation, Desalination 366 (2015) 113–120, http://dx.doi.org/10.1016/j.desal.2015.02.025.
[39] A. Piacentino, Application of advanced thermodynamics, thermoeconomics and exergy costing to a multiple effect distillation plant: in-depth analysis of cost formation process, Desalination 371 (2015) 88–103, http://dx.doi.org/10.1016/j.desal.2015.06.008.
[40] H.T. EL-Dessouky, H.M. Ettouney, F.A.L.J. Yhel, Multiple effect evaporation-vapour compression desalination processes, Trans. IChemE. 78 (2000) 662–676 0263-8762/00/$10.00+0.00.
[41] H.T. El-Dessouky, H.M. Ettouney, Fundamentals of Salt Water Desalination, first ed. Elsevier Science, 2002.
[42] H.T. El-Dessouky, H.M. Ettouney, Multiple-effect evaporation desalination systems: thermal analysis, Desalination 125 (1999) 259–276, http://dx.doi.org/10.1016/S0011-9164(99)00147-2.
[43] H.M. Ettouney, H.T. El-Dessouky, Al-Atiqi, Understand thermal desalination, Chem. Eng. Prog. 95 (1999) 43–54.
[44] H.M. Ettouney, Design of single-effect mechanical vapor compression, Desalination 190 (2006) 1–15, http://dx.doi.org/10.1016/j.desal.2005.08.003.
[45] F. Al-Juwayhel, H.T. El-Dessouky, H.M. Ettouney, Analysis of single-effect evaporator desalination systems combined with vapor compression heat pumps, Desalination 114 (1997) 253–275.
[46] J.M. Veza, Mechanical vapour compression desali- nation plants — a case study, Desalination 101 (1995) 1–10.
[47] M.A. Darwish, Thermal analysis of vapor compression desalination system, Desalination 69 (1988) 275–295.
[48] H.M. Ettouney, H.T. El-Dessouky, Y. Al-Roumi, Analysis of mechanical vapor compression desalination process, Int. J. Energy Res. 23 (1999) 431–451.
[49] N.H. Aly, A.K. El-Fiqi, Mechanical vapor compression desalination systems — case study, Desalination 158 (2003) 143–150.
[50] A. Karameldin, A. Lotfy, S. Mekhemar, The Red Sea area wind-driven mechanical vapor compression desalination system, Desalination 153 (2003) 47–53.
[51] H.S. Aybar, Analysis of a mechanical vapor com- pression desalination system, Desalination 142 (2002) 181–186.
[52] R. Bahar, M.N.A. Hawlader, L.S. Woei, Performance evaluation of a mechanical vapor compression desalination system, Desalination 166 (2004) 123–127.
[53] S. Mussati, N. Scenna, E. Tarifa, S. Franco, J.A. Hernandez, Optimization of the mechanical vapor compression (MVC) desalination process using mathematical programming, Desalin. Water Treat. 5 (2009) 124–131, http://dx.doi.org/10.5004/dwt.2009.572.
[54] K. Thu, Y.-D. Kim, M.W. Shahzad, J. Saththasivam, K.C. Ng, Performance investigation of an advanced multi-effect adsorption desalination (MEAD) cycle, Appl. Energy 159 (2015) 469–477, http://dx.doi.org/10.1016/j.apenergy.2015.09.035.
[55] H.W. Chung, J. Swaminathan, D.M. Warsinger, J.H. Lienhard, Multistage vacuum membrane distillation (MSVMD) systems for high salinity applications, J. Membr. Sci. 497 (2016) 128–141, http://dx.doi.org/10.1016/j.memsci.2015.09.009.
[56] A. Matsuda, K. Kansha, Y. Fushimi, C. Tsutsumi, A. Kishimoto, Advanced Energy Saving and its Applications in Industry, Springer, New York, 2013.
[57] I. Kemp, Pinch Analysis and Process Integration, Butterworth, 2007.
[58] H.T. El-Dessouky, H.M. Ettouney, F. Al-Juwayhel, Multiple effect evaporation—vapour compression desalination processes, Chem. Eng. Res. Des. 78 (2000) 662–676, http://dx.doi.org/10.1205/026387600527626.
[59] J.J.J. Chen, Comments on improvements on a replacement for the logarithmic mean, Chem. Eng. Sci. 42 (1987) 2488–2489, http://dx.doi.org/10.1016/0009-2509(87)80128-8.
[60] R. Smith, Chemical Process Design and Integration, second ed. John Wiley and Sons Ltd., England, 2005.
[61] R.C. Turton, R.C. Bailie, W.B. Whiting, Analysis, Synthesis, and Design of Chemical Processes, fourth ed., 2012.
[62] J.R. Couper, W.C. Penney, J.R. Fair, S.M. Walas, Chemical Process Equipment, Selection and Design, 2 second ed. Elsevier, USA, 2010.
[63] T. Hayes, Sampling and Analysis of Water Streams Associated With the Development of Marcellus Shale Gas, 10, Rep. by Gas Technol. Institute, Des Plaines, IL, 2009 Marcellus Shale Coalit.
[64] P. Slutz, J. Anderson, J. Broderick, R. Horner, Key shale gas water management strategies: an economic assessment tool, SPE/APPEA Int. Conf. Heal. Safety, Environ. Oil Gas Explor. Prod. Perth, Aust. (2012) Sept. 2012.
[65] R.D. Vidic, S.L. Brantley, J.M. Vandenbossche, J.D. Abad, Impact of shale gas development on regional water quality, Science 340 (2013).
[66] J. Zammerilli, A. Murray, R.C. Davis, T. Littlefield, Environmental Impacts of Unconventional Natural Gas Development and Production, 800, 2014 553–7681.
[67] A.S. Drud, CONOPT: A System for Large Scale Nonlinear Optimization, Reference Manual for CONOPT Subroutine Library, ARKI Consulting and Development A/S, Bagsvaerd, Denmark, 1996.
[68] I.E. Grossmann, J.A. Caballero, H. Yeomans, Advances in mathematical programming for the synthesis of process systems, Lat. Am. Appl. Res. 284 (2000) 263–284.
[69] G.P. Thiel, J.H.V. Lienhard, Treating produced water from hydraulic fracturing: composition effects on scale formation and desalination system selection, Desalination 346 (2014) 54–69, http://dx.doi.org/10.1016/j.desal.2014.05.001.
[70] Q. Jiang, J. Rentschler, R. Perrone, K. Liu, Application of ceramic membrane and ion-exchange for the treatment of the flowback water from Marcellus shale gas production, J. Membr. Sci. 431 (2013) 55–61, http://dx.doi.org/10.1016/j.memsci.2012.12.030.
[71] European Commission, Eurostat, 2016.